AD_____

AWARD NUMBER: W81XWH-06-1-0069

TITLE: Systemic and Gene Modified Mesenchymal Stem Cell Therapy for Metastatic
        Prostate Cancer

PRINCIPAL INVESTIGATOR: Selvarangan Ponnazhagan, Ph.D.

CONTRACTING ORGANIZATION: University of Alabama at Birmingham
                               Birmingham, AL 35294

REPORT DATE: May 2009

TYPE OF REPORT: Annual

PREPARED FOR: U.S. Army Medical Research and Materiel Command
               Fort Detrick, Maryland 21702-5012

DISTRIBUTION STATEMENT: Approved for Public Release;
                        Distribution Unlimited

The views, opinions and/or findings contained in this report are those of the author(s) and
should not be construed as an official Department of the Army position, policy or decision
unless so designated by other documentation.

REPORT DOCUMENTATION PAGE

Form Approved
OMB No. 0704-0188

1. REPORT DATE	2. REPORT TYPE	3. DATES COVERED
1 May 2009	Annual	1 May 2008 – 30 Apr 2009

4. TITLE AND SUBTITLE	
Systemic and Gene Modified Mesenchymal Stem Cell Therapy for Metastatic Prostate Cancer	**5a. CONTRACT NUMBER**
	5b. GRANT NUMBER W81XWH-06-1-0069
	5c. PROGRAM ELEMENT NUMBER

6. AUTHOR(S)	
Selvarangan Ponnashagan, Ph.D.	**5d. PROJECT NUMBER**
	5e. TASK NUMBER
E-Mail: pons@uab.edu	**5f. WORK UNIT NUMBER**

7. PERFORMING ORGANIZATION NAME(S) AND ADDRESS(ES)	8. PERFORMING ORGANIZATION REPORT NUMBER
University of Alabama at Birmingham Birmingham, AL 35294	

9. SPONSORING / MONITORING AGENCY NAME(S) AND ADDRESS(ES)	10. SPONSOR/MONITOR'S ACRONYM(S)
U.S. Army Medical Research and Materiel Command Fort Detrick, Maryland 21702-5012	
	11. SPONSOR/MONITOR'S REPORT NUMBER(S)

12. DISTRIBUTION / AVAILABILITY STATEMENT
Approved for Public Release; Distribution Unlimited

13. SUPPLEMENTARY NOTES

14. ABSTRACT

Bone is the frequent metastatic site for human prostate cancer resulting in significant morbidity and mortality in patients with advanced disease. The type of bone defect encountered in prostate cancer bone metastasis is osteoblast lesions resulting in excess bone. However, initiation of osteoclastogenesis is first aided by osteolysis, mediated by osteoclasts. The areas provided as source for osteoblast accumulation later leads to thickening of the bone. In this proposal, we planned to address arresting both the events of osteolysis and osteoblastogeneis by biological inhibitors of these two events. Osteoprotegerin (OPG) is a "decoy" receptor that competes with RANK for RANKL, thus, modulating the effects of RANKL. Thus, OPG remains an effective molecule for future therapies for bone metastasis. We sought to achieve sustained effects of OPG combining cell therapy and gene therapy approaches. Similarly, for inhibiting osteoblast activity we chose noggin, capable of arresting osteoblast formation. The aims were to determine therapeutic effects of OPG and noggin expression by rAAV gene therapy in a murine model of prostate cancer bone metastasis. So far, we completed studies with OPG by both intramuscular administration of a vector encoding OPG and by genetically-engineering mesenchymal stem cells (MSC) to express OPG for cell based therapy. Currently we are determining the role of AGR2, a protein identified to play a vital role in prostate cancer bone metastasis. For inhibiting osteoblast lesions, we have produced a vector encoding noggin and determined its therapeutic effects by intramuscular administration using a prostate cancer cell line known to produce osteoblast lesions. Studies using this vector-transduced MSC therapy did not provide significant therapy. We will identify the limitation and possibly overcoming them with alternate approaches. Additional studies to determine the role of AGR2 in prostate cancer bone metastasis will be performed.

15. SUBJECT TERMS
Osteolysis, osteoprotegerin, noggin, gene therapy, adeno-associated virus

16. SECURITY CLASSIFICATION OF:			17. LIMITATION OF ABSTRACT	18. NUMBER OF PAGES	19a. NAME OF RESPONSIBLE PERSON USAMRMC
a. REPORT U	**b. ABSTRACT** U	**c. THIS PAGE** U	UU	70	**19b. TELEPHONE NUMBER** *(include area code)*

Standard Form 298 (Rev. 8-98)
Prescribed by ANSI Std. Z39.18

Table of Contents

Title of the Grant: Systemic and gene modified mesenchymal stem cell therapy for metastatic prostate cancer
Award number: W81XWH-06-1-0069
Principal Investigator: Selvarangan Ponnazhagan, Ph.D.
Annual Report: April 01, 2008 – May 31, 2009

INTRODUCTION

Bone is the frequent metastatic site for human prostate cancer resulting in significant morbidity and mortality in patients with advanced disease. A vicious cycle, arising due to the interaction of cancer cells and the bone microenvironment results in the upregulation of factors promoting osteoblastogenesis. Presently, it is clear that the even t of osteoblastogenesis in prostate cancer bone m etastasis is preceeded by osteoclastogenesis. Thus, osteolysis and osteoblastogenesis can be inhibited by interrupting one or more of the steps involved in the cycle.

A better un derstanding of bone rem odeling and m olecular events in o steolytic and o steoblastic bone lesions identified the role of ke y activators and inhibitors of both the se events.   The receptor activator of nuclear factor κ B ligand (RANKL), produc ed by osteoblasts, activated T cells an d marrow stromal cells stimulates the recruitment, differentiation, and activation of osteoclasts by binding to RANK. Osteoprotegerin (OPG) is a "decoy" receptor that competes with RANK for RANKL thereby modulating the effects of RANKL. Thus, OPG is a prom ising m olecule for in hibiting osteoc lastogenesis. On the   other hand, noggin, a secreted glycoprotein with prove n antagonist ic activity o n bone m orphogenetic proteins (B MP) and   osteoblast differentiation will inhibi t osteoblastic lesions. To achieve sustained effects of these two m   olecules, gene therapy is m ore powe rful than pharm acological therapies. Sin ce bone m etastasis is a secondary ev ent that occurs in lat e-stage disea se or during recurrence, genetic therapies aim ed at controlling this proce ss should be sustained and localized. Thu s, for sustained e xpression of t herapeutic levels of OPG or no ggin, a vector capable of stable expression of the tra nsgene without vector-associated toxicity and imm unity is id eal. The adeno-associated virus vectors (AAV) are more promising to this end. With recombinant AAV, it is possible to obtain significant therapeutic gains by either system ic or bone-targeted transduction using mesenchymal stem cells with bone homing signals.

The central hy pothesis of the proposed wo   rk is that sy   stemic or bone targeted gene therapy   u sing recombinant AAV and   gene-m odified m esenchymal stem cell vehicles capable of bone hom   ing and inhibiting osteoclastic an d osteoblastic bone lesions in   prostate cancer by   stable expression of OPG and noggin respectively will be effective tr eatment modalities for prostate cancer bone metastasis. The proposed studies will seek to identify the effects of OPG and noggin therapy also as a means to delineate the in tricate role of osteoclastogenesis and osteoblastogenesis in the progression of prostate cancer bone metastasis. This hypothesis will be evaluated in the present   study by using a novel bone-targeted m esenchymal stem cell vehicle, and non-invasiv e biolum inescent im aging of the im   planted pr ostate cancer cell growth and metastases in SCID mouse.

Specific Aims: 1) To d evelop and characterize rAAV encodi ng human OPG and nog gin, and clones of PC-3, LAPC-9 and LNCaP cell lines stably expre ssing luciferase for non-inv asive im aging, 2) To determ ine preventive and therapeutic effects of system ic and bone-targeted OPG expression b y rAAV gene therapy in SCID m ice with osteoly tic, osteoblastic and   mixed lesions of prostate cancer bone m   etastasis, *and* 3) To determine preventive and therapeutic effects of B MP antagonist noggin b y rAAV gene therapy in metastatic prostate cancer mice models *in vivo*.

BODY

Progress reports of the past years on this work have provided details of the results from first two specific aims. We had begun work outlined in the 3 [rd] specific aim during the last year, producing rAAV encoding noggin for osteoblas lesions. Initial studies using this vector by intramuscular administration indicated significant bone restoration f ollowing challenge with 22Rv cell line.

Results of the micro-CT performed to determ ine skeletal structures of experimental animals, which indicated restoration of tibial indicated higher co rtical and trabecular bone de nsity (Figure 1) trabecular bone volum e and connectivity density (Figure 2) and cortical thickness (Figure 3) in MSC-noggin treated m ice compared to only MSC-GFP treated mice. All data a re reported as m ean ± standard deviation (SD). Bone m ineral density (BMD) and bone m ineral contents (BMC) were analyzed using ANOVA. Comparison of differences between tw o variables was perform ed using the two-tailed, two-sample with equal variances, independent t test.

When the vecto r was used to trans duce mesenchymal s tem cells for th e co mbination o f gene and cell therapy, however, the therapy effect was found to be only marginal. W e are currently determining if this is because of inadequate production of noggin by MS C or lack of sufficient quantities of genetically-engineered MSC at the site of osteoblast bone lesion. We will addres s this in the no-cost exte nsion pe riod
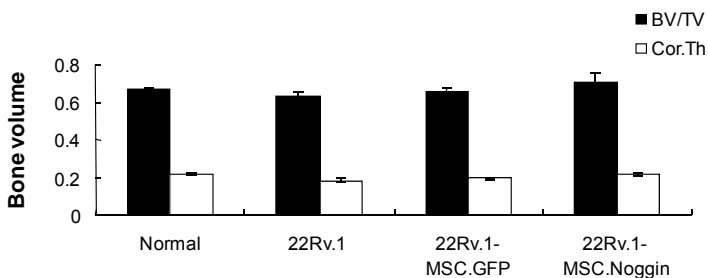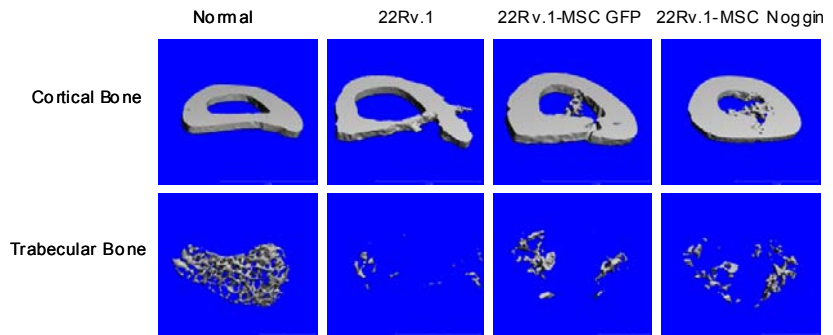

Figure 1. Micro-CT analysis f or cortical and trabecular b one architecture. 4-6 week old SCID male m ice were implanted in tra-tibially with 10^5 osteobl astic 22Rv.1 pro state cancer cells expressing firefly lu ciferase. Mice were imaged for bioluminescence and the tumors were allowed to grow f or 7days wh en 5×10^5 MSC expressing either GFP/Noggin were implanted in the tibia at the site of tumor inoculation. Mice were imaged for bioluminescence 4 weeks after the initiation of treatment and micro-CT was performed to determine skeletal structures of experimental animals, which indicated restoration of tibial bone in both MSC-GFP and MSC-Noggin treated mice. Higher trabecular bone volume and connectivity density were observed in MSC-Noggin treated mice compared to only MSC-GFP treated mice.
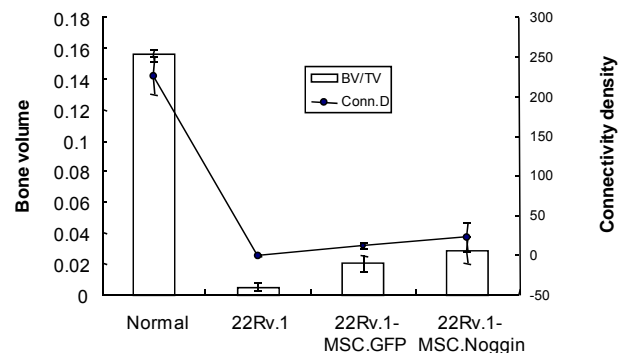

Figure 2. Bone volume and connectivity density of tibiae in normal mice and mice treated with MSC-GFP or MSC-noggin.

and m ake modif ications to incr ease eithe r the number of MSC (by seque ntial ad ministration) or expression level of noggin by using alternate AAV serotype capsids capable of high-efficiency gene transf er, that h ave been identified recently.

Interaction between PC3 cells and MSC *in vitro*: In o rder to de termine the inf luence of

Figure 3. Relative bone volume and cortical thickness of tibiae in normal mice and mice treated with MSC-GFP or MSC-noggin.

tumor cells and cells of the bone m arrow on bone dam age, PC3 cells were grown in three dim ensional spheroids on hu-biogel m atrices and co-culture d along with bone m arrow derived m ouse MSC in a trans-well plate in the presence or absence of bone m arrow conditi oned m edia. Aft er 72 hours of co-culture the PC3 spheroids were harvested and s ubjected to total RNA isola tion f ollowed by cDNA
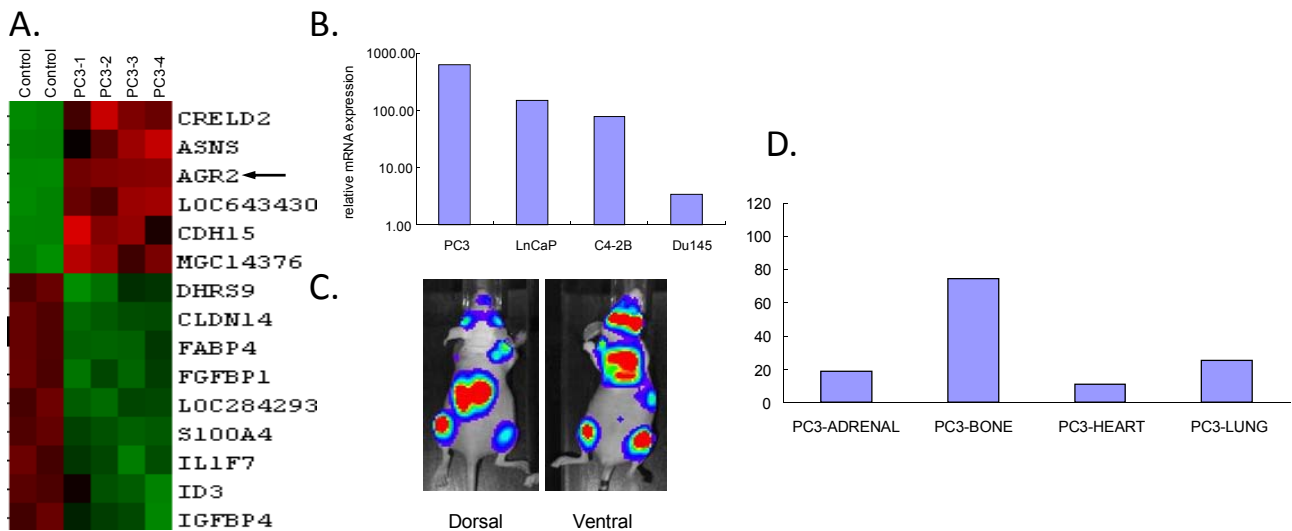

Figure 4: **A**. cDNA microarray heat map showing up-regulation of AGR2 expression in PC3 cells cultured in bone marrow conditioned media (arrow). **B**. RT-PCR analysis showing relative mRNA profile in various prostate cancer cell lines derived from bone (PC3, C4-2B), lymph node (LnCap) and brain metastases (Du145). **C**. Bioluminescence imaging showing metastases of PC3 cells after intra-cardiac inoculation in 6 week-old SCID male mice (1-300 sec). **D**. PC3 cells were harvested from different metastatic location from SCID mice, grown in culture, RNA isolated and subjected to RT-PCR analysis for AGR2 expression.

microarray analysis for changes in gene expression. Results indicated significan t increase in anterior gradient (AGR2) expression in the PC3 cells cultured in presence of MSC and bone marrow conditioned media when com pared to PC3 cells grown in re gular m edia without the MSC. AGR2 over-expression was further confirm ed by real tim e PCR analysis. To test th e im plication of AGR2 in prosta te c ancer bone metastasis, total R NA was isolated from various prostate cancer bone m etastatic cell lines (PC3, LnCap, C4-2B) and a brain m etastatic cell line (Du145) to analyze for AGR2 expression by R T-PCR. Data indicated Du145 has the least am ount of AGR2 expression com pared to the bone m etastatic cell lines; PC3 showing the highest expr ession and thus suggesting that AGR 2 m ight play an im portant in the event(s) of bone metastasis. To further investigate the involvement of AGR2 in bone metastasis, PC3 cells expressing firefly luciferase was inje cted into the lef t ventricle o f heart in a thymic nude m ice (n=2). Metastases were confirmed in lung, heart, bone (tibia) an d the adrenal glands. PC3 tum or cells were rescued from those organs and grown in cultu re, RNA isolated and test ed for AGR2 expression. Highest amount of AGR2 expression was obtained from the cells derived from tibial bone, strengthening importance of AGR2 in bone metastasis (Figure 4).

Lentivirus expressing short hairpin RNA was used to silence AGR2 in the PC3 cells to evaluate the growth of PC3 cells *in vivo*. Athymic nude mice were injected either subcutaneously or intra-tibially or intra-cardiac with 10 [6] PC3 cells with silenced AGR2. Tum or progression was checked by bioluminescence imaging and results indicated com plete absence of tumor growth in m ice injected with AGR2 silenced PC3 cells com pared to norm al PC3 cells (Figure 5). W e are currently trying to create a PC3 cell line carrying a non-target shRN A sequence to make sure that inhibition of tumor growth is due to AGR2 silencing rather than lentiviral integration into the genome.
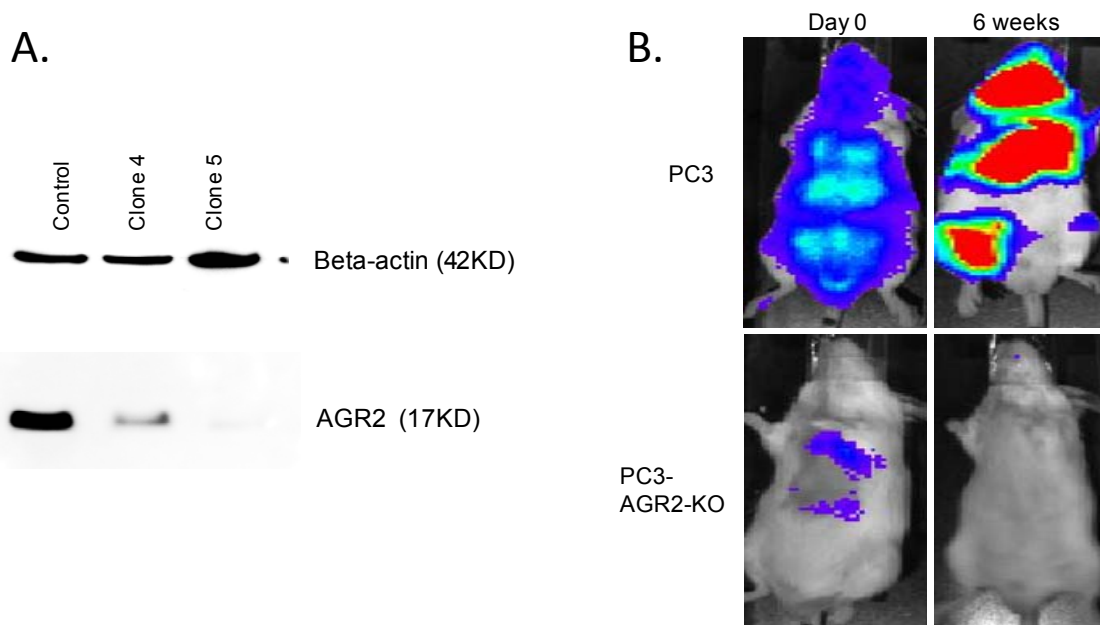
Figure 5: **A**. Western-Blot analysis for AGR2 expression in PC3 cells and PC3 cells with AGR2 knockdown. **B**. Bioluminescence imaging indicating AGR2 knock out PC3 cells failed to develop tumor in SCID mice compared to regular PC3 cells.

KEY RESEARCH ACCOMPLISHMENTS

- Demonstrated that intramuscular adm inistration of rAAV encoding noggin provides therapy effects following challenge with the human prostate cancer cell line 22Rv.1.
- However, therapy effects of MSC, genetically engineered to produce noggin did not provide significant outcome. Current studies are aimed at identifying the limitation and possibly overcoming them with alternate approaches.
- Identified that AGR2 expression plays a significant role in prostate cancer growth in the bone.

REPORTABLE OUTCOMES
(Papers published or communicated)

Isayeva., T., Moore, L .D., Chanda, D., Chen, D ., and Ponnazhagan, S. Tum oristatic effects of endostatin in prostate cancer is dependent on androgen receptor status. The Prostate 2009 69:1055-66.

Chanda D, Isayeva T, K umar S, Hensel JA, Sawant A, Ram aswamy G, Siegal GP, and Ponnazhagan, S.. Therapeutic potential of adult st em cells for osteolytic bone m etastasis. Clinical Cancer Res. 2009 (in press).

Kumar S, Wan, C, Ra maswamy G, Clem ens, TL, a nd Ponnazhagan, S. Modified m esenchymal stem cells producing osteogenic and angiogenic factors enhance bone regeneration in a m ouse m odel of segmental bone defect. Mol. Ther. 2009 (communicated).

CONCLUSIONS

In the last year of funding we developed and validated rAAV encoding noggin in preventing osteoblastic bone defect in athym ic nude m ice with hum an prosta te cancer cells in the bone, capable of producing

osteoblastic bone phenotype. Stud ies using this vector-transduced MSC therapy did not provide significant therapy. We will identify the lim itation and possibly ov ercoming them with alternate approaches. Additional studies to determine the role of AGR2 in prostate cancer bone metastasis will be performed.

PERSONNEL RECEIVING PAY FROM THIS GRANT
Selvarangan Ponnazhagan, Ph.D.
Diptiman Chanda, Ph.D.

REFERENCES
N/A

APPENDICES
Two papers attached.

Tumoristatic Effects of Endostatin in Prostate Cancer Is Dependent on Androgen Receptor Status

Tatyana Isayeva,[1] Lakisha D. Moore,[1] Diptiman Chanda,[1] Dongquan Chen,[2] and Selvarangan Ponnazhagan[1]*

[1]*Department of Pathology, The University of Alabama at Birmingham, Birmingham, Alabama*
[2]*Department of Medicine, The University of Alabama at Birmingham, Birmingham, Alabama*

BACKGROUND. Although anti-angiogenic therapy is a promising new line of therapy for prostate cancer, we recently reported that stable expression of endostatin arrested the progression of prostate cancer to poorly differentiated state and distant metastasis in TRAMP mice. However, the same therapy failed to provide any benefit when given either during or after the onset of metastatic switch. The present study determined the possible mechanisms behind the selective advantage of endostatin therapy in early-stage disease.
METHODS. Angiogenesis-related gene expression analysis was performed to identify target genes and molecular pathways involved in the therapy effects. Based on the results from in vivo studies, and recapitulation of the in vivo data in vitro using tumorigenic and non-tumorigenic human prostate cancer cells that are either androgen-sensitive or androgen-independent, analyses of possible mechanisms of the selective advantage of early treatment were performed using assays for cell proliferation, apoptosis, migration, and cell signaling. The identified mechanisms were further confirmed in vivo.
RESULTS. Results indicated that cells with high androgen receptor (AR) expression were more sensitive to endostatin treatment than androgen-independent cells with low or no AR expression. Endostatin was found to significantly downregulate the expression of growth factors, receptor tyrosine kinases, proteases, and AR both in vitro and in vivo only when the cells express high-levels of AR. Cell proliferation was not influenced by endostatin treatment but migration was significantly affected only in androgen-sensitive cells. Targeted downregulation of AR prior to endostatin treatment in androgen-sensitive cells and overexpression of AR in androgen-independent cells indicated that the effect of endostatin via AR downregulation is mediated by a non-genotropic mechanism on Ras and RhoA pathways, and independently of AR on MAPK/ERK pathway.
CONCLUSIONS. These data indicate that systemically stable endostatin expression delays the onset of metastatic switch by acting on multiple pathways involving AR. *Prostate 69: 1055– 1066, 2009.* © 2009 Wiley-Liss, Inc.

KEY WORDS: prostate cancer; metastasis; androgen receptor; anti-angiogenesis; TRAMP model

INTRODUCTION

Prostate cancer is the second leading cause of cancer deaths in American men [1]. In the last few years, studies have identified several molecular events that occur during the development of more aggressive, androgen-independent tumor, leading to the development of targeted therapies for the management of the disease [2–5]. Among promising new therapies for prostate cancer, anti-angiogenic therapy is aimed at arresting the formation of new blood vessels from

pre-existing vascular bed, which is crucial for the progression of tumor growth, invasion, and metastasis.

Despite promising preclinical studies, translation of anti-angiogenic therapy in human patients has yielded very limited success [6,7]. Most of the patients in these clinical trials exhibited end-stage disease with poorly differentiated tumors [8–10]. Our recent studies in the transgenic adenocarcinoma mouse prostate (TRAMP) model indicated that sustained systemic levels of endostatin and angiostatin did not eliminate the tumor growth but greatly delayed the progression of the disease into high-grade prostatic intraepithelial neoplasia (PIN) and well-differentiated tumor, only when initiated prior to the onset of metastatic process, suggesting the existence of possible limitations of this therapy for late-stage disease [11]. The present study determined the molecular mechanisms that regulate the selective advantage of this therapy prior to metastatic switch. Results of this study indicated the role of androgen receptor (AR) signaling in endostatin effects observed in early-stage disease. Molecular profiling of prostate tissue from TRAMP mice following endostatin therapy and recapitulation of the in vivo data using androgen-sensitive and androgen-independent prostate cancer cells indicated a significant downregulation of growth factors known to promote cell invasion and migration. Proteins of Ras, RhoA, and MAPK/ERK pathways were downregulated only in cells with high AR levels. There was a significant decrease in AR levels following endostatin treatment. Further, AR ablation studies indicated a direct effect of endostatin on Src kinase and by an indirect, non-genotropic effect of AR on Ras and RhoA suggesting the involvement of signaling events regulating AR on the effects of endostatin therapy during androgen-dependent and androgen-independent stages of prostate cancer. Overexpression of AR in AR-negative, androgen-independent prostate cancer cells also resulted in inducing the effects of endostatin observed in AR-positive, androgen-sensitive cells. Collectively, these data provide new insight to improve the effects of anti-angiogenic therapy for late-stage prostate cancer.

MATERIALS AND METHODS

Cells and Reagents

The human embryonic kidney cell line 293 and human prostate cancer cell lines LNCaP, C4-2, Du145, LNCaP, and PC3 were purchased from ATCC and grown in RPMI 1640 medium (Gibco). All antibodies were purchased from Cell Signaling Technology, Inc. (Beverly, MA). The expression vector for human AR was obtained from OriGene Technologies, Inc.,

Rockville, MD. AR-specific and control siRNA were purchased from Santa Cruz Biotechnology, Inc. (Santa Cruz, CA).

Transgenic Mice

Transgenic males and non-transgenic littermates were obtained as TRAMP C57BL/6 × FVB Breeder F_1. Genotyping for the probasin-Tag transgene was performed by PCR using DNA isolated from tail biopsy [12]. Animal care and treatments were conducted in accordance with established guidelines and protocols approved by the University of Alabama at Birmingham Institutional Animal Care Committee.

Treatment and Analysis of Tissues

Details of the anti-angiogenic therapy in TRAMP mice have been published recently [11]. Cell morphology and histology of tumor sections were evaluated in H&E stained formalin-fixed tissue. All prostate lobes, including anterior, ventral, and dorsolateral lobes, were reviewed by an experienced pathologist in a blinded fashion and graded. Prostate lesions were scored using a 1–6 scale that has been established for TRAMP mice [13].

Gene Expression Analysis Using Angiogenesis-Specific Microarray

RNA from prostate tissues was isolated using the TRIzol method (Invitrogen). RNA from at least five mice were included from each group for each time point for the microarray analysis. Biotin-UTP-labeled cRNA probe was synthesized using 10 µg of purified total RNA and reverse transcriptase (TrueLabeling-AMP 2.0 Kit; S.A. Bioscience Corp., Frederick, MD). Six micrograms of purified cRNA from each sample was then incubated with an Oligo GEArray® Mouse Angiogenesis Microarray (OMM-024, Superarray, Inc.). The hybridized arrays were washed and detected with chemiluminescence according to the manufacturer's instructions (G.E. Array, Bethesda, MD). Signals were captured on films and scanned at 300 DPI in TIFF format, and analyzed by the GEArray analysis suite (Superarray, Inc.). Standardization of all signals was performed by normalizing the raw data with that of GAPDH.

Effects of Endostatin Treatment on Prostate Cancer Cells

LNCaP, C4-2, PC3, and Du145 cells were treated with recombinant endostatin or BSA at a concentration of 1 µg/ml for 60 min. Then, cells were harvested for cell lysate or RNA preparation, or used for

proliferation, apoptosis, and migration assays described below.

Real-Time PCR

Total RNA was isolated using the TRIzol reagent (Invitrogen). A two-step quantitative real-time, reverse transcription-PCR (RT-PCR) was performed on cDNA generated using the iScript cDNA Synthesis Kit and iQ SYBR Green Supermix (Bio-Rad). The levels of target gene expression were calculated after normalization with GAPDH levels. Normalized expression was determined using the comparative C_t method, and fold changes were derived from the $2^{-\Delta\Delta C_t}$ values for each gene [14]. Sequences of the primers used in RT-PCR reactions are given in Table I.

Immunohistochemistry

Immunohistochemical studies were performed in 5 μm sections of paraffin-embedded tumor tissues using antibodies for AR, anti-PARP p85. Ras, ERK, RhoA, Src, and cytokeratin-8. Antigen retrieval was achieved by incubating the slides in 0.05% trypsin for 20 min at 37°C. Secondary antibodies were respective, isotype-matched, anti-mouse or anti-rabbit antibodies

TABLE I. Sequences of Primers Used in RT-PCR

hAR	F.P. 5′-AAGACGCTTCTACCAGCTCACCAA-3′
	R.P. 5′-TCCCAGAAAGGATCTTGGGCACTT-3′
mAR	F.P. 5′-TCAAGGGAGGTTACGCCAAAGGAT-3′
	R.P. 5′-ACAGAGCCAGCGGAAAGTTGTAGT-3′
hADRA2b	F.P. 5′-TCATCATGGGCACTTTCACCCTCT-3′
	R.P. 5′-AGCTCCTGGAAGGCAATCCTGAAA-3′
hEGFR	F.P. 5′-TTTGCCAAGGCACGAGTAACAAGC-3′
	R.P. 5′-ATTCCCAAGGACCACCTCACAGTT-3′
mEGFR	F.P. 5′-CATTGATGGCCCACACTGTGTCAA-3′
	R.P. 5′-TACCCAGATGGCCACACTTCACAT-3′
hEphrinA2	F.P. 5′-TCTCGGAGAAGTTCCAGCTCTTCA-3′
	R.P. 5′-TATTGCTGGTGAAGATGGGCTCAG-3′
hEphrinA3	F.P. 5′-AACGTGCTGGAAGACTTTGAGGGA-3′
	R.P. 5′-AGGCCAAGAACGTCATGAGGAAGA-3′
hEphrinA2R	F.P. 5′-CGTGTGGAGCTTTGGCATTGTCAT-3′
	R.P. 5′-AGCACTGCATCATGAGCTGGTAGA-3′
hEphrinA3R	F.P. 5′-TGGAGCAGGTGAATTTGGAGAGGT-3′
	R.P. 5′-ATGCTTGCTTCTCCCAGGAAGTCT-3′
hGAPDH	F.P. 5′-TCGACAGTCAGCCGCATCTTCTTT-3′
	R.P. 5′-ACCAAATCCGTTGACTCCGACCTT-3′
mGAPDH	F.P. 5′-TCAACAGCAACTCCCACTCTTCCA-3′
	R.P. 5′-ACCCTGTTGCTGTAGCCGTATTCA-3′
hMDK	F.P. 5′-AGCCAAGAAAGGGAAGGGAAAGGA-3′
	R.P. 5′-AAGCTAACGAGCAGACAGAAGGCA-3′
hMMP-9	F.P. 5′-TGGGCTACGTGACCTATGACAT-3′
	R.P. 5′-GCCCAGCCACCTCCACTCCTC-3′
hMMP-2	F.P. 5′-GAAGGTGAAGGTCGGAGT-3′
	R.P. 5′-GAAGATGGTGATGGGATTTC-3′
hNrp-1	F.P. 5′-TAACGACCCACTCTGCTTCTTGCT-3′
	R.P. 5′-TTGCCAAATCTTCAGAGCCCTTGC-3′
hPleiotrophin	F.P. 5′-TGTGGATACTGCTGAAGCAGGGAA-3′
	R.P. 5′-GGGTCTTCATGGTTTGCTTGCACT-3′
hPI3K p110	F.P. 5′-ATCCCAGGTGGAATGAATGGCTGA-3′
	R.P. 5′-AATGGAAAGGCAAAGTCGAGCAGC-3′
mN-Ras	F.P. 5′-TCCTAGCTGGCCTCAAACTCACAA-3′
	R.P. 5′-TCAGTCAGGTGTGTGTGGTGGAAT-3′
mH-Ras	F.P. 5′-AGTCCGTGAGATTCGGCAGCATAA-3′
	R.P. 5′-GGACAGCACACATTTGCAGCTCAT-3′
mK-Ras	F.P. 5′-AGACACGAAACAGGCTCAGGAGTT-3′
	R.P. 5′-TAGAAGGCATCGTCAACACCCTGT-3′

conjugated to HRP or Alexa Fluor, and were used at a dilution of 1:500.

Analysis of Cell Signaling

Immunoblotting was performed as described in Ref. [14]. Briefly, cell extracts from prostate cancer cells were separated in 10% SDS–PAGE gels and then transferred onto nitrocellulose membranes. Detection of specific proteins was performed using antibodies for pERK1/2, ERK1/2, Ras, pSrc, Src, pAKT, AKT, RhoA, and β-actin. Blots were developed with ECL reagent obtained from Amersham Pharmacia Biotech (Piscataway, NJ). Protein bands were detected by chemiluminescence (Pierce).

Cell Proliferation, Apoptosis, and Migration Assays

For cell proliferation, cells were seeded in 96-well plates (6×10^2 cells/well) and allowed to attach overnight. The cells were incubated in serum-free medium for 24 hr, and then treated with 1 µg/ml of recombinant endostatin for 1 hr. Cell proliferation was measured 24, 48, and 72 hr later using the Celltiter 96 Aqueous One Solution Cell Proliferation Assay kit (Promega) according to the manufacturer's protocol. For apoptosis assay, 100 µl of the cell suspensions (10^5 cells) were incubated with 5 µl Annexin V and 5 µl propidium iodine for 15 min, in the dark, at room temperature and analyzed by Flow cytometry. For migration assay, cells were plated as 10^5 cells/well in a 6-well plate coated with fibronectin. The cells were serum-starved for 12 hr following which 10 µg/ml mitomycin C was added to the media for 2 hr. Next, the cells were treated with purified endostatin for 1 hr and a ''wound'' created using a sterile 200 µl pipette tip. Photographs of the wounded area were taken at the time of wounding and thereafter every 24 hr for 3 days to determine the rate of wound closure. Percent migration was calculated by measuring the width of the cell-free in five points along the scratch and then averaged.

Modulation of AR in Human Prostate Cancer Cells

Abrogation of AR was performed by siRNA transfection using the Transfection reagent (Santa Cruz Biotechnology, Inc.) and constitutive AR overexpression was achieved by transfecting the AR expression vector using Lipofectamin 2000 (Invitrogen). Transfections were performed 24 hr prior to the treatment of cells with endostatin, either using purified protein or by transfecting subsequently an expression vector for endostatin. The cells were harvested and lysates prepared and analyzed as before.

Data Analysis

For the analysis of microarray data, the GEarray software (S.A. Biosciences) was used. The Pathway Architect software (Agilent, CA) was used for pathway analysis and annotation. The Superarray images were uploaded onto the GEarrays software, and minimum signal was used as background. Signal medium was used for signal intensity and Student's t-test for statistical analysis. Only a differential gene expression of >2-fold was considered significant. The gene lists obtained by filtering both P-value and fold changes were used for pathway analysis and annotation. Analysis of gene expression results containing two or more groups was done using the Student's t-test, assuming equal variance. Student's t-test was used to determine statistical significance in all other experimental data. Values of $P < 0.05$ were considered statistically significant.

RESULTS

Molecular Profiling of Angiogenesis-Related Gene Expression in the Prostate Tissue of TRAMP Mice Following Anti-Angiogenic Therapy

Towards understanding the possible mechanisms behind the selective advantage of systemically stable anti-angiogenic therapy only in early-stage disease, gene expression analysis was performed to identify differentially expressed angiogenesis-related genes from prostate tissues of naïve and treated mice with tumor grades 3, 4, 5, and 6. Results of this study is given in Figure 1A.

Following endostatin therapy, there was a significant downregulation in the expression of genes involved in migration, cell growth, and apoptosis as shown in Figure 1A. Downregulation of growth factors, FGF, Mdk, PDGF, Ptn, TGFβ1 and TGFβ3, tyrosine kinase receptors Ffgr3 and Nrp1, and proteinases MMP2, MMP9 was observed when the treatment was given during androgen-sensitive stages of the disease. At the stage of prostatic intraepithelial hyperplasia, only Akt1 expression was similar in naïve mice compared to the treated group. The major mechanism of Akt activation is through PI3 kinase pathway [15]. Ephrin (Efna2, Efna3) expression was slightly increased in the stage of neoplasia and continued to increase three times in well-differentiated tumors and six times in poorly differentiated tumors of naïve mice. Ephrin receptors have been implicated in the process of metastasis by activating the Rho signaling pathway and reorganization of cytoskeletal elements [16,17]. Mice that received endostatin and angiostatin treatment showed a significant decrease in Ephrins, especially Efna 3, which was restricted to basal levels.
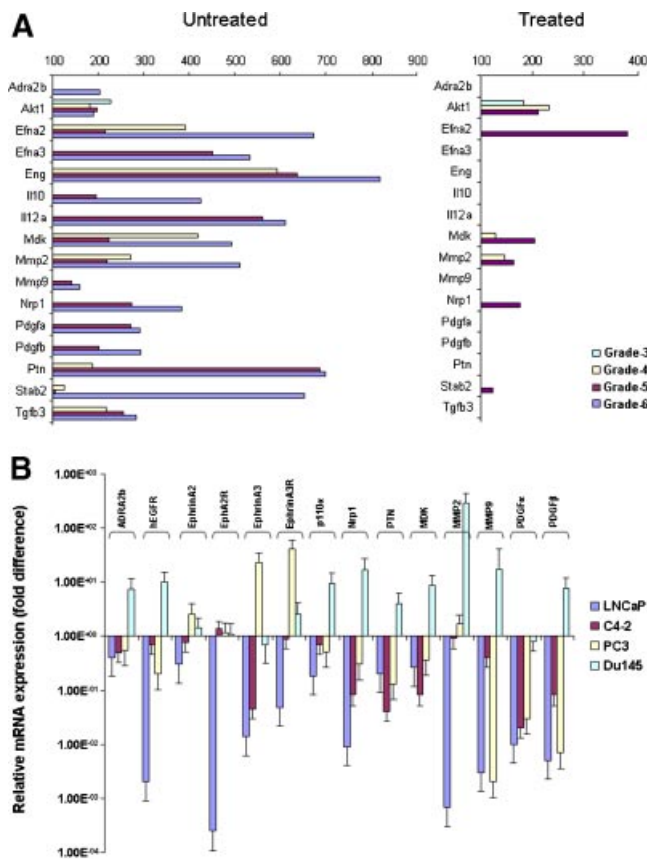
Fig. 1. A: Differential expression of angiogenesis-related genes during prostate cancer progression in naïve TRAMP mice and following endostatin and angiostatin therapy. Following confirmation of tumor grade, RNA was isolated from prostate tissues of untreated (**left panel**) and treated (**right panel**) mice and used for microarray analysis with Oligo GEArray® Mouse Angiogenesis array. Relative increase/decrease in the expression of indicated genes was based on comparison with values obtained in the prostate tissue of age-matched, non-transgenic littermates, taken as 100. Different colors in each bar represents tumor grade. Grade-3: high-prostatic intraepithelial neoplasia (PIN); Grade- 4: well-differentiated tumor; Grade-5: moderately differentiated tumor; Grade- 6: poorly differentiated tumor. **B**: Analysis of gene expression in human prostate cancer cells following endostatin treatment. Androgen-sensitive (LNCaP) and androgen-independent (C4-2, PC3, and Dul45) human prostate cancer cells were treated with endostatin for 1 hr and RNA was isolated. Relative expression of indicated genes was analyzed by RT-PCR and values represented in comparison to levels in untreated cells indicated as the midpoint.

Angiogenic Gene Expression Profile was More Pronounced in the Transition Stage of Well-Differentiated Tumor to Moderately Differentiated Tumor

Five genes namely *Efna2*, *Eng*, *Mdk*, *MMP2*, *TGFβ3* were highly expressed ($P < 0.003$) in well-differentiated prostate tumors in untreated mice compared to

mice treated with endostatin and angiostatin. Endoglin (CD105) is a membrane protein involved in the TGF-β receptor-signaling pathway with predominant expression in proliferating endothelial cells [18,19]. There was a significant downregulation of midkine family growth factors, Mdk and Ptn following endostatin treatment ($P < 0.003$). During tumor progression, the number of highly expressed genes in naïve group was broadly increased compared to the treated group ($P < 0.05$). These included genes involved in extracellular matrix degradation (MMP2, MMP9, TIMP2), angiogenesis (Adra2b, Ecgf1, Efna2, Efna3, Nrp1, Pofut1, PDGF, and FGF), and cell proliferation and metastasis (MAPK14, Ptn, Pecam1, PDGF, FGF). None of these genes were found to be in significant numbers in the prostate tissue of normal, transgene-negative littermates.

Determination of Endostatin Effects in Androgen-Sensitive and Androgen-Independent Human Prostate Cancer Cells

Since genes that were downregulated in the prostate tissues of treated mice were associated with cell signaling and kinase activation, which promote cell growth, migration, and activation of cancer cell signaling by paracrine and autocrine mechanisms, characteristic of the transitional stage of prostate cancer cells becoming androgen-independent, we designed studies to understand the associated molecular events following endostatin treatment in androgen-sensitive and androgen-independent human prostate cancer cells. First, we independently tested the effects of endostatin, angiostatin, and the combination of both endostatin and angiostatin, and observed maximum effects in endostatin and endostatin plus angiostatin groups. Hence, further efforts have focused on endostatin as the anti-angiogenic factor.

Initially, we performed studies to confirm recapitulation of the effects observed in gene expression analysis of prostate tissues from TRAMP mice, treated with endostatin. Briefly, androgen-sensitive LNCaP cells and androgen-independent C4-2, Du145, and PC3 cells were treated with endostatin for 1 hr. RNA was isolated from the cells and relative expression of key genes, which were downregulated in vivo following endostatin therapy, were analyzed by RT-PCR. Results, shown in Figure 1B, indicated a similar pattern of downregulation of gene expression only in the androgen-sensitive (LNCaP) and AR overexpressing (C4-2) human prostate cancer cells. This observation was identical to that observed in gene expression analysis from prostate tissue of TRAMP mice, given therapy at early-stage disease. Based on clustering of genes according to pathways regulating cell function, we

further characterized the effects of endostatin treatment on proliferation, migration, apoptosis, cell signaling, and RT-PCR.

Downregulation of MAPK/ERK Signaling in AR-Positive Cells Following Endostatin Treatment

By immunoblotting, we determined that treatment with endostatin significantly inhibited pERK expression in DHT-stimulated LNCaP and C4-2 cells (Fig. 2A). However, there was no decrease in pAKT following endostatin treatment in any of the cells. ERK signaling pathways are involved in cell proliferation, differentiation, actin cytoskeleton reorganization, and cell migration. Moreover, ERKs are also involved in stress response and cell death [20–22]. However, there was no effect of endostatin on ERK activity in Du145 and PC3 cells, which are androgen-independent and express no or low-level AR, respectively. One of the important targets for ERK is IkB kinase-α [23,24]. We found a significant decrease in pIkB-α level in the endostatin-treated LNCaP and C4-2 cells (data not shown). Endostatin has been shown to activate Src in endothelial cells through association with $\alpha_5\beta_1$ integrin and caveolin-1 [25]. Upregulation of integrin and caveolin-1 has been implicated in human prostate cancer progression/metastasis and shown to promote cancer cell survival [26–28]. Thus, we determined whether treatment of endostatin exerts differential effects on Src activity in androgen-sensitive and androgen-independent cells. Interestingly, data from our studies indicated a significant decrease in pSrc in androgen-dependent LNCaP and AR overexpressing C4-2 cells following endostatin treatment. In contrast, pSrc level was increased in the androgen-independent cell lines Du145 and PC-3 following endostatin treatment (Fig. 2A).

Endostatin Treatment Does Not Influence Proliferation but Decreases Migration of Prostate Cancer Cells

Results, shown in Figure 2B, indicated that there was no significant effect of endostatin on proliferation in
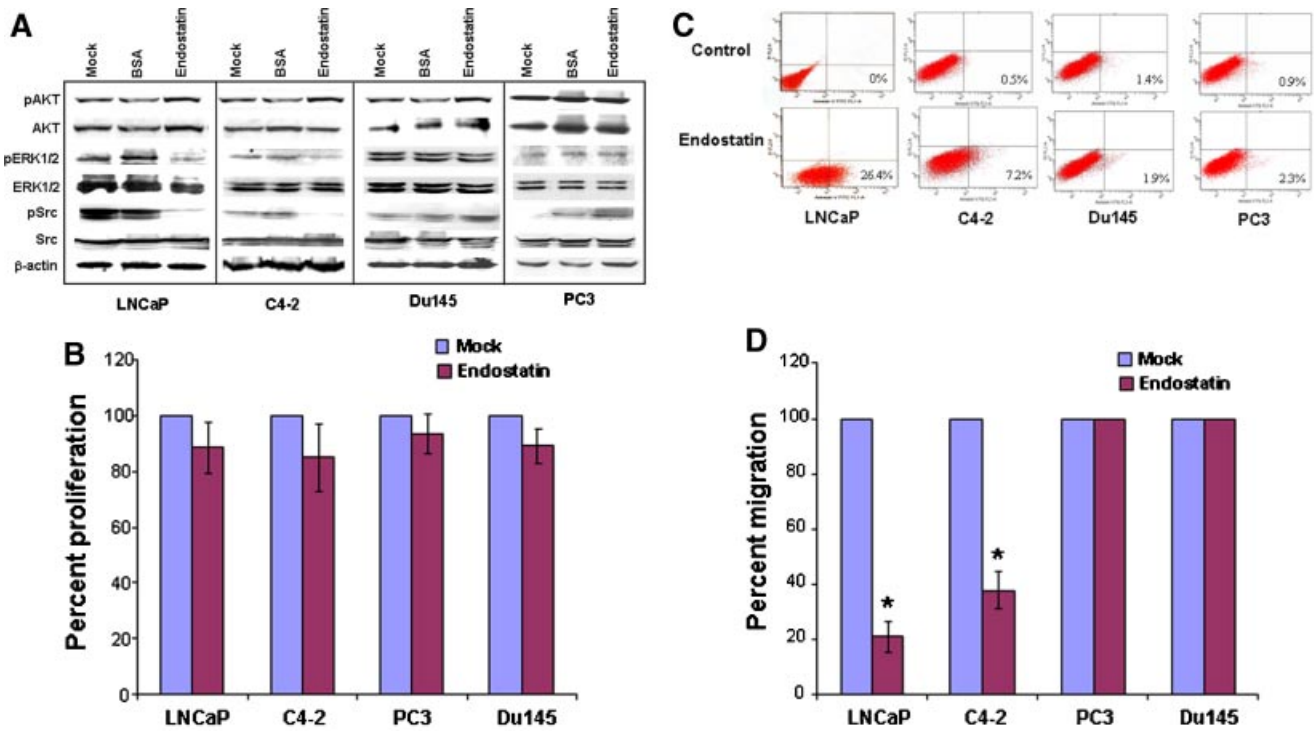

Fig. 2. Effects of endostatin on kinase activation, proliferation, apoptosis, and migration in androgen-sensitive and androgen-independent prostate cancer cell lines. Androgen-sensitive (LNCaP) and androgen-independent (C4-2, PC3, and Du145) human prostate cancer cells were either mock-treated or treated with BSA or purified recombinant endostatin for 1 hr. Following treatments, the cells were lysed in cold lysis buffer supplemented with proteinase and phosphatase inhibitors. Cell lysates containing equal amount of protein were resolved by 10% SDS–PAGE, transferred to nitrocellulose membrane, and detected with indicated antibodies (**A**). Cells were incubated with 10 nM DHT for 16 hr followed by treatment with 1 μg/ml endostatin for 1 hr. Cell proliferation was measured by CellTiter 96 One Solution Cell Proliferation Assay (**B**). Apoptosis was measured using annexin V-FITC Apoptosis Detection Kit. All assays were performed in triplicate (**C**). Cells were analyzed for cell migration using the wound-healing scratch assay. Cells were "wounded" and monitored every 24 hr for 3 days to determine the rate of migration into the scratched area (**D**) (*P < 0.001).

any of the cells. The results of apoptosis indicated no effects following endostatin treatment in androgen-independent prostate cancer cells although there was approximately 25% apoptosis in the androgen-sensitive LNCaP cells at earlier time point (Fig. 2C). However, migration showed a significant decrease following endostatin treatment in AR-overexpressing LNCaP and C4-2 cells ($P < 0.0003$; Fig. 2D). Interestingly, migration was not affected in Du145 or PC3 cells following endostatin treatment (Fig. 2D).

Downregulation of Ras and RhoA in Endostatin Treated Prostate Cancer Cells

Ras and RhoA are two proteins of Ras superfamily of small GTP-binding proteins, which play a central role in actin cytoskeleton organization, oncogenic transformation, and adhesion. RhoA also plays an important role in proliferation and migration as well as motility and invasiveness of human prostate cancer [29,30]. From the above results on AR overexpressing cells that endostatin did not affect proliferation but significantly decreased migration and also downregulated MAPK/ERK, we determined the status of Ras and RhoA in endostatin treated cells. Data from these studies are given in Figure 3. There was a significant repression of Ras and RhoA in LNCaP and C4-2 cells after treatment with soluble endostatin. In contrast, endostatin treatment increased the level of Ras and RhoA in androgen-independent DU145 and PC3 cells (Fig. 3).

Downregulation of Activated ERK, Src, Ras, and RhoA in Prostate Tissue of Endostatin Treated TRAMP Mice

From the results obtained in vitro, we inferred that a possible arrest in migration of AR overexpressing cells is mediated through suppression of ERK, Ras, and RhoA activities. To confirm whether the same mechanism was responsible for delaying tumor progression

Fig. 3. Ras and RhoA activities following endostatin treatment of human prostate cancer cells. Androgen-sensitive (LNCaP) and androgen-independent (C4-2, PC3, and Du145) human prostate cancer cells were either mock-treated or treated with BSA or recombinant endostatin for 1 hr. Following treatments, the cells were lysed in cold lysis buffer supplemented with proteinase and phosphatase inhibitors. Cell lysates containing equal amount of protein were resolved on 10% SDS–PAGE, transferred to nitrocellulose membrane, and probed with Ras and RhoA antibodies.

and arrest of metastasis in vivo, ERK, RhoA, and Ras were analyzed from prostate tissues of treated and untreated TRAMP mice by RT-PCR and immunohistochemistry. Data, shown in Figure 6, indicated a significant decrease of pErk in the treated group compared to naïve mice. Staining for activated ERK was not permanent but foci of ERK were observed in prostatic intraepithelial hyperplasia lesions and in well-differentiated tumors of naïve mice (Fig. 4A). In the prostate lobes of endostatin treated mice, pERK expression was much lower in all stages of tumor progression. Immunoreactivity of RhoA was high in well-differentiated stage of prostate tumor form naïve TRAMP mice and was very weak in endostatin treated group (Fig. 4A). Similar to RhoA, Ras expression was found to be significantly high in the prostate lobes of naïve mice with well-differentiated tumors but the expression was significantly reduced following the therapy (Fig. 4B). Analysis of the expression of the three closely related Ras genes *HRas*, *KRas*, and *NRas* by RT-PCR indicated significant increase of HRas in high-grade PIN in naïve mice. However, following endostatin treatment the HRas level was significantly reduced ($P < 0.05$). KRas activity was highest in the well-differentiated tumors (grade-5) of untreated mice. However, following the therapy, the level of KRas was significantly reduced. There was no significant difference in NRas between naïve and endostatin treated mice (Fig. 4C). Staining of well-differentiated tumor with pSrc antibody indicated significantly higher levels in naïve mice but endostatin treatment during early stages of the disease greatly decreased pSrc in well-differentiated tumors despite the fact that progression to well-differentiated state was greatly delayed following early treatment. However, pSrc level was comparable in mice treated at late-stage to the untreated naïve group (Fig. 4D).

Expression of AR in Prostate Cancer Cells In Vivo and In Vitro After Endostatin Treatment

Since several of the observed changes following endostatin treatment were found more in prostate cancer cells with high AR expression both in vitro and in TRAMP mice in vivo, we next determined whether the observed effects of endostatin negatively influence AR expression. Prostate cancer cells were stimulated with DHT and then treated with endostatin, and AR expression in LNCaP, C4-2, and PC3 cells was determined. Results, shown in Figure 5A, indicated a significant decrease in AR expression in LNCaP and C4-2 cells after culturing in the presence of endostatin ($P < 0.001$). Similarly, RT-PCR using RNA form the prostate tissue of naïve and endostatin treated mice, and immunohistochemistry of prostate tissues showed
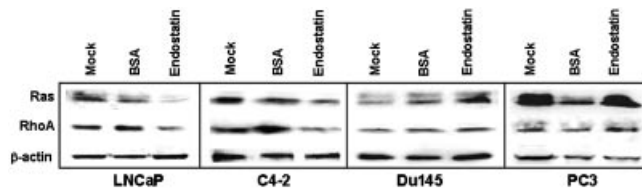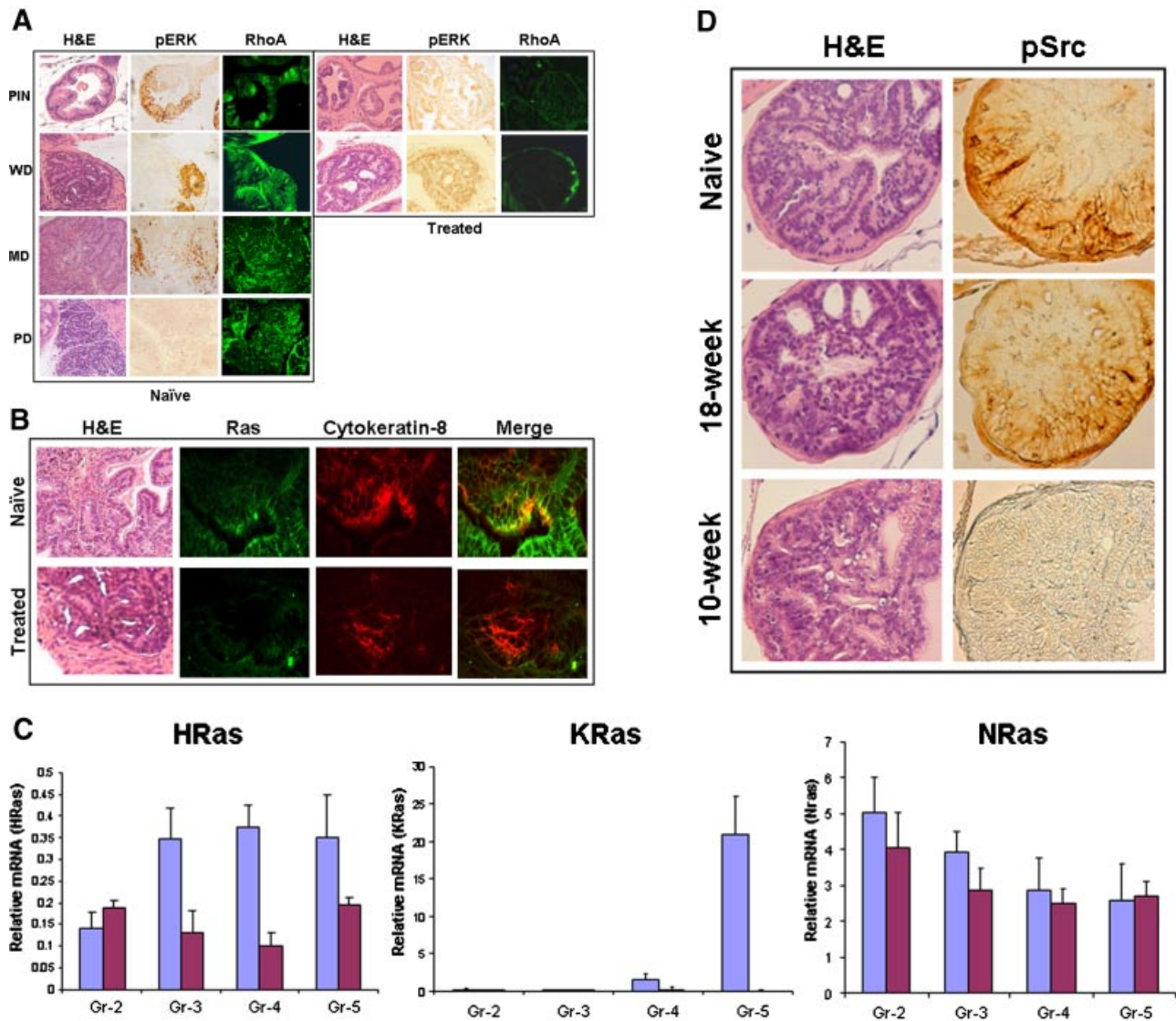
Fig. 4. Erk, RhoA, Ras and Src levels in the prostate tissue of untreated and endostatin treated TRAMP mice. **A**: pErk and RhoA were detected in the prostate tissues of untreated TRAMP mice with prostatic intraepithelial neoplasia (PIN), well-differentiated (WD), moderately differentiated (MD), and poorly differentiated (PD) tumors, and in PIN and WD tumors of treated mice. **B**: Ras expression in naïve and treated mice was analyzed in WD tumors and cancer cells identified by counterstaining with cytokeratin-8. **C**: RT-PCR analysis of HRas, KRas, and NRas in the prostate tissues of naïve and endostatin treated mice. Bars indicate mean values from samples obtained from five mice in each group for each tumor grade (*$P < 0.05$). **D**: pSrc expression in naïve mice or mice that were given treatment at 10 or 18 weeks of age was determined when the animals were 24 weeks old. H&E staining was performed for each antibody staining to confirm the location of immunoreactive regions of the prostate.

a significant downregulation of AR in the treated group (Fig. 5B,C; $P < 0.001$).

Targeted Abrogation of AR In Situ Reverses the Effects of Endostatin Function

To determine whether the observed effects on kinase activities are associated with AR function or effected independently of AR, targeted abrogation of AR using siRNA was performed prior to endostatin treatment in LNCaP, C4-2, and Du145 cells. Results, shown in Figure 6A, indicated that only Src activity was found to be decreased whether AR expression was blocked or not in LNCaP and C4-2 cells. However, pSrc level remained unchanged in Du145 and PC3 cells whether AR siRNA was used or not prior to endostatin treatment. Abrogation of AR expression reversed the downregulation of RhoA and Ras to normal levels. Phospho-ERK level was decreased following AR siRNA transfer and further decreased in combination
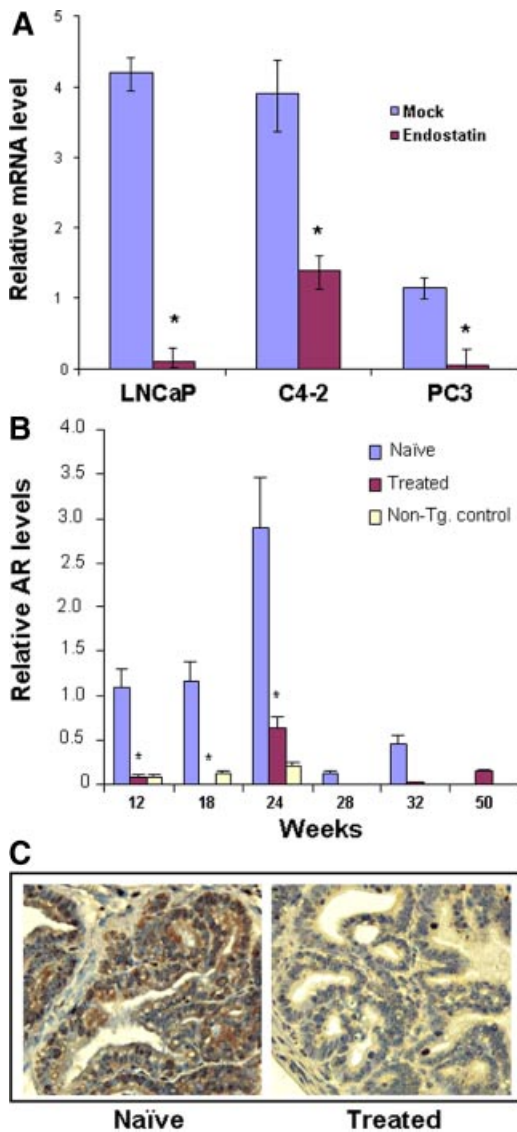
Fig. 5. Expression of AR in human prostate cancer cells and in prostate tissues of TRAMP mice following endostatin treatment. Total RNA was isolated from indicated prostate cancer cells (**A**) and from prostate tissues of non-transgenic control, untreated TRAMP mice, and those treated with endostatin (*P < 0.001 compared to mock). **B**: Quantitation of AR mRNA was performed by RT-PCR. Values from individual samples were normalized with respective GAPDH values (*P < 0.001 compared to naïve). **C**: Prostate tissue sections of naïve and treated TRAMP mice, obtained at 24 weeks of age, were stained immunohistochemically with AR antibody.

Fig. 6. Kinase activity in androgen-sensitive and androgen-independent human prostate cancer cells following modulation of AR and endostatin treatment. **A**: AR-positive LNCaP and C4-2, and AR-negative Du145 cells were transfected with endostatin expression vector following AR siRNA transfection. Cell lysates were prepared 24 hr later and analyzed for indicated signaling proteins by immunoblot. **B**: Du145 cells were transfected with an expression plasmid for AR. Twenty-four hours later, the cells were transfected with the endostatin expression vector. Cell lysates were prepared 24 hr after that and analyzed for indicated signaling proteins by immunoblot.

with endostatin treatment in LNCaP and C4-2 cells (Fig. 6A). However, endostatin treatment alone, even in the absence of AR blocking, decreased pERK levels greatly in these cells suggesting that the effect of endostatin on pSrc is independent of AR but down-regulation of AR influences the phosphorylation of ERK. Interestingly, pERK was also decreased in the
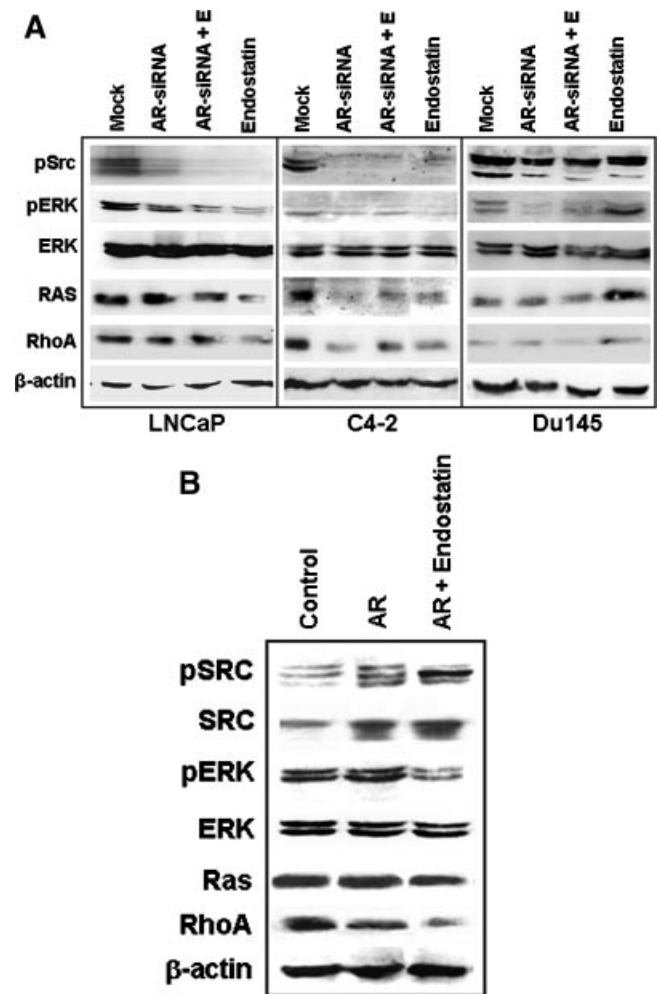
androgen-independent Du145 cells following AR blocking but as noted before, treatment with endostatin alone increased pERK in these cells (Fig. 6A).

Overexpression of AR in Androgen-Independent Prostate Cancer Cells Restores Endostatin Effects to That Seen in Androgen-Sensitive Cells

To confirm the significance of high-AR levels on the effects of endostatin, Du145 cells, which do not express detectable levels of AR, were transfected with an AR expression vector. After confirming high levels of AR

expression, the cells were either mock-transfected or transfected with a plasmid encoding endostatin. Later, lysates from these cells were tested by Western blot for cell signaling. Results of these studies, shown in Figure 6B, indicated that upon overexpression of AR, there was a significant downregulation of RhoA and pERK but not pSrc.

DISCUSSION

Despite promising preclinical studies that established safety and absence of systemic and organ toxicity, patient response to endostatin therapy for late-stage tumors has encountered little success [31–33]. Our recent studies in TRAMP mice, treated with endostatin and angiostatin, indicated that the treatment was highly effective for early-stage disease but there was no significant benefit when administered after the onset of metastatic switch [11]. Results of the present study indicate that in addition to inhibiting the growth of endothelial cells in the tumor environment, endostatin exerts a profound effect on prostate cancer cells directly. Initial characterization indicated activation of Akt and Erk signaling in early lesions of prostatic neoplasia in untreated TRAMP mice. Foci of activated Erk have been observed in the PIN lesion and well-differentiated tumors. Combined activation of Akt and Erk pathways stimulates epithelial AR function and blocks apoptosis-inducing paracrine signals from the stroma, leading to androgen-independent cancer [34,35]. When endostatin treatment was given at early-stage disease, there was a significant decrease in Erk, RhoA, Ras and Src activities. This was accompanied by a decrease in AR levels. AR plays a dual role in prostate cancer progression. The AR may also interact with or regulate multiple other proteins that can affect cell growth [36–38]. Results of the present study indicate that downregulation of molecular signals involved during the progression of prostate cancer, when the cancer cells become androgen-independent, exert profound anti-tumor effects following endostatin treatment. This appears to involve mainly kinases and growth factors that influence AR signaling. Downregulation of these molecules prior to metastatic switch of the disease greatly impacts on AR signaling, which shifts the homeostasis of the primary tumor to an aggressive metastatic disease, when the cells become androgen-independent, as well decrease the expression of AR.

Recapitulation of the data from in vivo studies using androgen-sensitive and androgen-independent prostate cancer cells indicated that endostatin treatment results in the downregulation of a number of growth factors and receptor tyrosine kinases mainly in androgen-sensitive and AR-overexpressing cells. The effect was more pronounced in Erk, Ras, and RhoA levels. Additionally, there was a concomitant decrease in proteases and growth factors including MMP2, MMP9, PCAM-1, FGF1, EGFR, MDK, and Ephrins.

The major pathways involved in the development of androgen escape of prostate cancer cells are MAPK and PI3K pathways. These pathways act to directly modify the AR, altering its sensitivity to both androgens and anti-androgens [39–41]. The observation that there was no decrease in pAKT following endostatin treatment in both androgen-sensitive and androgen-independent cells suggests that endostatin does not function through the PI3K signaling pathway. Thus, signaling through AKT, most commonly encountered in androgen-independent stages, may not be affected by endostatin, which partly accounts for the lack of its therapeutic effects on late-stage tumors. Analysis of Ras expression from the prostate tissues of treated animals and further characterization of the three closely related *Ras* genes indicated a significant decrease in HRas and KRas when the treatment was given at early stage of the disease. Decreased levels of Rho activity inhibit cell migration through disruption of cell–matrix interactions, reducing membrane ruffling and tail-retraction of migratory cells, and delaying the turnover of actin stress fibers and focal adhesions [42–44]. Similarly, in prostate cancer, enhanced expression of Ras protein has been shown to correlate with increased tumor grade [45,46].

Targeted abrogation of AR by siRNA in androgen-dependent and AR-positive cells reversed the effect of endostatin on RhoA, and Ras whereas pERK was not restored. This suggests that downregulation of AR by endostatin may cause a non-genotropic effect [36,47,48], indirectly, on MAPK pathway involving Ras and RhoA whereas direct inhibitory action of endostatin on ERK may be independent of AR downregulation. Further support for this mechanism was apparent when the androgen-independent Du145 cells, with no detectable AR expression, was transfected to overexpress AR and treated with endostatin, there was a significant downregulation of RhoA but not other kinases. This observation also suggests a possible influence of endostatin on AR to effect downregulation of RhoA by non-genotropic mechanism, and activation of AR by non-androgen ligands, when the prostate cancer cells acquire androgen-independent stage, may further cause inability of endostatin action in late-stage tumors. The observation that PC3 cells, which are androgen-independent, and express low-level AR did not show the observed effects of endostatin also prompts us to speculate that in addition to the effects of autocrine signaling by non-androgen ligands, the amount of AR expression may be an additional requirement for the treatment response to endostatin.

Results of in vitro and in vivo studies also indicate that downregulation of AR signaling also impacts on the transactivation of AR target genes. Impairment of AR signaling affects the autocrine production of growth factors that activate key signaling pathways. Decrease in the expression of EGFR, FGFR, VEGFR2, and PDGF following endostatin treatment provides support to this cascade. Once the prostate cancer cells acquire androgen-independent state, activation of AR by cytokines and peptide growth factors, produced by both tumor and non-tumor cells in the microenvironment, is likely to elicit various signaling network for continued proliferation, survival, and metastasis, independent of endostatin effects.

From the data obtained in C4-2 cells, which are androgen-independent, yet have high-level AR expression, it is also possible that intracellular trafficking of endostatin might be different in AR-sensitive and AR-independent cells. C4-2 are derived from LNCaP cells, which are androgen-sensitive. Interestingly, signaling effects observed in these cells were identical to that seen in LNCaP cells following endostatin treatment unlike in Du145 and PC3 cells, the other androgen-independent cells with relatively undetectable and low AR expression respectively. It will be of further interest to determine whether additional events such as variation in intracellular trafficking of endostatin also contribute to the difference in treatment effects.

Collectively, these studies suggest that while endostatin therapy may prove to be highly useful in early stages of the disease, combining endostatin with other therapies may be required for anti-tumor effects in late-stage prostate cancer.

ACKNOWLEDGMENTS

REFERENCES

1. Jemal A, Siegel R, Ward E, Hao Y, Xu J, Murray T, Thun MJ. Cancer statistics, 2008. CA Cancer J Clin 2008;58:71–96.

2. Dhanasekaran SM, Barrette TR, Ghosh D, Shah R, Varambally S, Kurachi K, Pienta KJ, Rubin MA, Chinnaiyan AM. Delineation of prognostic biomarkers in prostate cancer. Nature 2001;412:822–826.

3. Stamey TA, Warrington JA, Caldwell MC, Chen Z, Fan Z, Mahadevappa M, McNeal JE, Nolley R, Zhang Z. Molecular genetic profiling of Gleason grade 4/5 prostate cancers compared to benign prostatic hyperplasia. J Urol 2001;166:2171–2177.

4. Rhodes DR, Barrette TR, Rubin MA, Ghosh D, Chinnaiyan AM. Meta-analysis of microarrays: Interstudy validation of gene expression profiles reveals pathway dysregulation in prostate cancer. Cancer Res 2002;62:4427–4433.

5. Ashida S, Nakagawa H, Katagiri T, Furihata M, Iiizumi M, Anazawa Y, Tsunoda T, Takata R, Kasahara K, Miki T, Fujioka T, Shuin T, Nakamura Y. Molecular features of the transition from prostatic intraepithelial neoplasia (PIN) to prostate cancer: Genome-wide gene-expression profiles of prostate cancers and PINs. Cancer Res 2004;64:5963–5972.

6. Dahut WL, Scripture C, Posadas E, Jain L, Gulley JL, Arlen PM, Wright JJ, Yu Y, Cao L, Steinberg SM, Aragon-Ching JB, Venitz J, Jones E, Chen CC, Figg WD. A phase II clinical trial of sorafenib in androgen-independent prostate cancer. Clin Cancer Res 2008;14:209–214.

7. Bergers G, Hanahan D. Modes of resistance to anti-angiogenic therapy. Nat Rev Cancer 2008;8:592–603.

8. Logothetis CJ, Wu KK, Finn LD, Daliani D, Figg W, Ghaddar H, Gutterman JU. Phase I trial of the angiogenesis inhibitor TNP-470 for progressive androgen-independent prostate cancer. Clin Cancer Res 2001;7:1198–1203.

9. Kerr DJ. Targeting angiogenesis in cancer: Clinical development of bevacizumab. Nat Clin Pract Oncol 2004;1:39–43.

10. Kumar NB, Krischer JP, Allen K, Riccardi D, Besterman-Dahan K, Salup R, Kang L, Xu P, Pow-Sang J. A phase II randomized, placebo-controlled clinical trial of purified isoflavones in modulating steroid hormones in men diagnosed with localized prostate cancer. Nutr Cancer 2007;59:163–168.

11. Isayeva T, Chanda D, Kallman L, Eltoum IE, Ponnazhagan S. Effects of sustained anti-angiogenic therapy in multistage prostate cancer in TRAMP model. Cancer Res 2007;67:5789–5797.

12. Greenberg NM, DeMayo F, Finegold MJ, Medina D, Tilley WD, Aspinall JO, Cunha GR, Donjacour AA, Matusik RJ, Rosen JM. Prostate cancer in a transgenic mouse. Proc Natl Acad Sci USA 1995;92:3439–3443.

13. Suttie A, Nyska A, Haseman JK, Moser GJ, Hackett TR, Goldsworthy TL. A grading scheme for the assessment of proliferative lesions of the mouse prostate in the TRAMP model. Toxicol Pathol 2003;31:31–38.

14. Moore LD, Isayeva T, Siegal GP, Ponnazhagan S. Silencing of transforming growth factor-beta1 in situ by RNA interference for breast cancer: Implications for proliferation and migration in vitro and metastasis in vivo. Clin Cancer Res 2008;14:4961–4970.

15. Lin J, Adam RM, Santiestevan E, Freeman MR. The phosphatidylinositol 3′-kinase pathway is a dominant growth factor-activated cell survival pathway in LNCaP human prostate carcinoma cells. Cancer Res 1999;59:2891–2897.

16. Brantley-Sieders DM, Caughron J, Hicks D, Pozzi A, Ruiz JC, Chen J. EphA2 receptor tyrosine kinase regulates endothelial cell migration and vascular assembly through phosphoinositide 3-kinase-mediated Rac1 GTPase activation. J Cell Sci 2004;117:2037–2049.

17. Fang WB, Ireton RC, Zhuang G, Takahashi T, Reynolds A, Chen J. Overexpression of EPHA2 receptor destabilizes adherens junctions via a RhoA-dependent mechanism. J Cell Sci 2008;121:358–368.

18. Svatek RS, Karam JA, Roehrborn CG, Karakiewicz PI, Slawin KM, Shariat SF. Preoperative plasma endoglin levels predict biochemical progression after radical prostatectomy. Clin Cancer Res 2008;14:3362–3366.

19. Dallas NA, Samuel S, Xia L, Fan F, Gray MJ, Lim SJ, Ellis LM. Endoglin (CD105): A marker of tumor vasculature and potential target for therapy. Clin Cancer Res 2008;14:1931–1937.

20. Seger R, Krebs EG. The MAPK signaling cascade. FASEB J 1995;9:726–735.

21. Chang L, Karin M. Mammalian MAP kinase signalling cascades. Nature 2001;410:37–40.

22. Johnson GL, Lapadat R. Mitogen-activated protein kinase pathways mediated by ERK, JNK, and p38 protein kinases. Science 2002;298:1911–1912.

23. Lee FS, Peters RT, Dang LC, Maniatis T. MEKK1 activates both IkappaB kinase alpha and IkappaB kinase beta. Proc Natl Acad Sci USA 1998;95:9319–9324.

24. Nemoto S, DiDonato JA, Lin A. Coordinate regulation of IkappaB kinases by mitogen-activated protein kinase kinase kinase 1 and NF-kappaB-inducing kinase. Mol Cell Biol 1998; 18:7336–7343.

25. Wickstrom SA, Alitalo K, Keski-Oja J. Endostatin associates with integrin α5β1 and caveolin-1, and activates Src via a tyrosyl phosphatase-dependent pathway in human endothelial cells. Cancer Res 2002;62:5580–5589.

26. Thompson TC, Timme TL, Li L, Goltsov A. Caveolin-1, a metastasis-related gene that promotes cell survival in prostate cancer. Apoptosis 1999;4:233–237.

27. Bartz R, Zhou J, Hsieh JT, Ying Y, Li W, Liu P. Caveolin-1 secreting LNCaP cells induce tumor growth of caveolin-1 negative LNCaP cells in vivo. Int J Cancer 2008;122:520–525.

28. Tahir SA, Yang G, Goltsov AA, Watanabe M, Tabata K, Addai J, Fattah el MA, Kadmon D, Thompson TC. Tumor cell-secreted caveolin-1 has proangiogenic activities in prostate cancer. Cancer Res 2008;68:731–739.

29. Itoh K, Yoshioka K, Akedo H, Uehata M, Ishizaki T, Narumiya S. An essential part for Rho-associated kinase in the transcellular invasion of tumor cells. Nat Med 1999;5:221–225.

30. Somlyo AV, Phelps C, Dipierro C, Eto M, Read P, Barrett M, Gibson JJ, Burnitz MC, Myers C, Somlyo AP. Rho kinase and matrix metalloproteinase inhibitors cooperate to inhibit angiogenesis and growth of human prostate cancer xenotransplants. FASEB J 2003;17:223–234.

31. O'Reilly MS, Boehm T, Shing Y, Fukai N, Vasios G, Lane WS, Flynn E, Birkhead JR, Olsen BR, Folkman J. Endostatin: An endogenous inhibitor of angiogenesis and tumor growth. Cell 1997;88:277–285.

32. Thomas JP, Arzoomanian RZ, Alberti D, Marnocha R, Lee F, Friedl A, Tutsch K, Dresen A, Geiger P, Pluda J, Fogler W, Schiller JH, Wilding G. Phase I pharmacokinetic and pharmacodynamic study of recombinant human endostatin in patients with advanced solid tumors. J Clin Oncol 2003;21:223–231.

33. Kulke MH, Bergsland EK, Ryan DP, Enzinger PC, Lynch TJ, Zhu AX, Meyerhardt JA, Heymach JV, Fogler WE, Sidor C, Michelini A, Kinsella K, Venook AP, Fuchs CS. Phase II study of recombinant human endostatin in patients with advanced neuroendocrine tumors. J Clin Oncol 2006;24:3555–3561.

34. Ghosh PM, Malik S, Bedolla R, Kreisberg JI. Akt in prostate cancer: Possible role in androgen-independence. Curr Drug Metab 2003;4:487–496.

35. Kinkade CW, Castillo-Martin M, Puzio-Kuter A, Yan J, Foster TH, Gao H, Sun Y, Ouyang X, Gerald WL, Cordon-Cardo C, Abate-Shen C. Targeting AKT/mTOR and ERK MAPK signaling inhibits hormone-refractory prostate cancer in a preclinical mouse model. J Clin Invest 2008;118:3051–3064.

36. Unni E, Sun S, Nan B, McPhaul MJ, Cheskis B, Mancini MA, Marcelli M. Changes in androgen receptor nongenotropic signaling correlate with transition of LNCaP cells to androgen independence. Cancer Res 2004;64:7156–7168.

37. Linja MJ, Porkka KP, Kang Z, Savinainen KJ, Jänne OA, Tammela TL, Vessella RL, Palvimo JJ, Visakorpi T. Expression of androgen receptor coregulators in prostate cancer. Clin Cancer Res 2004;10:1032–1040.

38. Léotoing L, Manin M, Monté D, Baron S, Communal Y, Lours C, Veyssière G, Morel L, Beaudoin C. Crosstalk between androgen receptor and epidermal growth factor receptor-signalling pathways: A molecular switch for epithelial cell differentiation. J Mol Endocrinol 2007;39:151–162.

39. Uzgare AR, Isaacs JT. Enhanced redundancy in Akt and mitogen-activated protein kinase-induced survival of malignant versus normal prostate epithelial cells. Cancer Res 2004;64:6190–6199.

40. Araki S, Omori Y, Lyn D, Singh RK, Meinbach DM, Sandman Y, Lokeshwar VB, Lokeshwar BL. Interleukin-8 is a molecular determinant of androgen independence and progression in prostate cancer. Cancer Res 2007;67:6854–6862.

41. Wang Y, Kreisberg JI, Ghosh PM. Cross-talk between the androgen receptor and the phosphatidylinositol 3-kinase/Akt pathway in prostate cancer. Curr Cancer Drug Targets 2007;7:591–604.

42. Ridley AJ, Comoglio PM, Hall A. Regulation of scatter factor/hepatocyte growth factor responses by Ras, Rac, and Rho in MDCK cells. Mol Cell Biol 1995;15:1110–1122.

43. Nobes CD, Hall A. Rho GTPases control polarity, protrusion, and adhesion during cell movement. J Cell Biol 1999;144:1235–1244.

44. Santos MF, McCormack SA, Guo Z, Okolicany J, Zheng Y, Johnson LR, Tigyi G. Rho proteins play a critical role in cell migration during the early phase of mucosal restitution. J Clin Invest 1997;100:216–225.

45. Viola MV, Fromowitz F, Oravez S, Deb S, Finkel G, Lundy J, Hand P, Thor A, Schlom J. Expression of ras oncogene p21 in prostate cancer. N Engl J Med 1986;314:133–137.

46. Agnantis NJ, Constantinidou AE, Papaevagelou M, Apostolikas N. Comparative immunohistochemical study of ras-p21 oncoprotein in adenomatous hyperplasia and adenocarcinoma of the prostate gland. Anticancer Res 1994;14:2135–2140.

47. Kousteni S, Bellido T, Plotkin LI, O'Brien CA, Bodenner DL, Han L, Han K, DiGregorio GB, Katzenellenbogen JA, Katzenellenbogen BS, Roberson PK, Weinstein RS, Jilka RL, Manolagas SC. Nongenotropic, sex-nonspecific signaling through the estrogen or androgen receptors: Dissociation from transcriptional activity. Cell 2001;104:719–730.

48. Kousteni S, Chen JR, Bellido T, Han L, Ali AA, O'Brien CA, Plotkin L, Fu Q, Mancino AT, Wen Y, Vertino AM, Powers CC, Stewart SA, Ebert R, Parfitt AM, Weinstein RS, Jilka RL, Manolagas SC. Reversal of bone loss in mice by non-genotropic signaling of sex steroids. Science 2002;298:843–846.

Therapeutic potential of adult bone marrow-derived mesenchymal stem cells in prostate cancer bone metastasis

Diptiman Chanda[1], **Tatyana Isayeva**[1], **Sanjay Kumar**[1], **Jonathan A. Hensel**[1], **Anandi Sawant**[1]**, Girish Ramaswamy**[2], **Gene P. Siegal**[1], **Matthew S. Beatty**[1] and **Selvarangan Ponnazhagan**[1*]

Department of Pathology[1], and Biomedical Engineering[2]

The University of Alabama at Birmingham

Birmingham, AL 35294

Corresponding author

Selvarangan Ponnazhagan, Ph.D.

Department of Pathology

701, 19th Street South, LHRB 513

The University of Alabama at Birmingham

Birmingham, AL 35294-0007

Phone: (205) 934-6731; Fax: (205) 975-9927

E-mail: pons@uab.edu

Statement of Translational Relevance

Osteolytic bone damage is major cause of morbidity in several cancers. Due to the refractory nature of metastatic tumors in the bone, conventional chemotherapy combinations and radiation therapy fail to provide long-term cure. Further, even the modes effects offered by these therapies fail to restore bone destruction. Thus, new therapies are needed for the management of osteolytic bone damage in cancer patients. Results of the present study demonstrate that without any genetic modification, adult mesenchymal stem cells (MSC) are capable of inducing bone formation in response to cancer-associated bone loss. Since MSC are immune privileged, and their use in allogenic context has entered human clinical trials, results of this preclinical study is greatly poised as a potential alternative for cancer-induced bone damage not only for prostate cancer bone metastasis, which initiates with osteolytic events but also other cancers such carcinomas of the breast, thyroid, lung, kidney and myeloma.

ABSTRACT

Purpose: Current evidence indicates that an osteoblast lesion in prostate cancer is preceded by osteolysis. Thus, prevention of osteolysis would reduce complications of bone metastasis. Bone marrow-derived mesenchymal stem cells (MSC) have the ability to differentiate into osteoblast, and produce osteoprotegerin (OPG), a decoy receptor for the receptor activator for nuclear factor κ B ligand (RANKL), naturally. The present study examined the potential of unmodified MSC to prevent osteolytic bone lesions in a preclinical mouse model of prostate cancer.

Experimental design: The human prostate cancer cell line PC3 was implanted in tibiae of SCID mice. After establishment of the tumor, either unmodified or genetically-engineered MSC overexpressing OPG was injected at the site of tumor growth. The effects of therapy were monitored by bioluminescence imaging, micro-CT, immunohistochemistry and histomorphometry.

Results: Data indicated significant (*P<0.001*) inhibition of tumor growth and restoration of bone in mice treated with both unmodified and modified MSC. Detailed analysis suggested that the donor MSC inhibited tumor progression by producing woven bone around the growing tumor cells in the tibiae and by preventing osteoclastogenesis.

Conclusions: Overcoming the limitation of the number of MSC available in the bone can provide significant amelioration for osteolytic damage without further modification.

INTRODUCTION

Prostate cancer is the second leading cause of cancer deaths in men behind lung cancer in the United States and metastasizes to bone in more than 70% of the cases during advance stages (1). Bone metastasis causes severe bone pain, pathological fractures and shortens life span by significant amount. Majority of the bone metastatic cancers (breast, lung, thyroid and kidney) generates osteolytic lesions whereas prostate cancer generates osteoblastic phenotype with an overall increase in bone volume (2-4). However, the appearance of osteoblastic lesions is preceded and/or accompanied by an osteolytic event, which is required for the establishment and growth of prostate cancer cells in the bone microenvironment (4, 5). The binding of receptor activator of nuclear factor-κB ligand (RANKL) to RANK on preosteoclasts or osteoclasts is essential for their maturation and activity (6, 7). Increased expression of RANKL has been observed in osteolytic malignancies and inhibition of osteoclastogenesis or metastasis has been considered as an intervention strategy. Osteoprotegerin (OPG) is a soluble decoy receptor for RANKL and prevents binding of RANKL to RANK, leading to inhibition of osteoclast activity and bone metastasis (8- 10). OPG therefore promises tremendous hope for potential clinical use in the management of osteolytic bone metastasis. Systemic delivery of OPG has shown promise as a potential therapy in animal models, limiting hypercalcemia and osteolysis induced by myeloma, breast, lung or prostate cancer and reducing tumor establishment in bone (11-17).

Homing of adult bone marrow derived mesenchymal stem cells (MSC) to the sites of tumor growth is well known besides their ability to self-renew and differentiate into bone, cartilage, fat and of other tissue types (18). Systemic administration of MSC in mice has been shown to engraft within the tumor microenvironment in many cancers and thus represent an attractive cellular vehicle for cell therapy and gene therapy (19, 20). Since OPG is constitutively

produced by MSC, we speculated that lack of MSC in sufficient quantities in the bone microenvironment is the reason for the inability to inhibit excess osteoclastogenesis and compensate for bone loss, and overcoming this limitation would provide therapy for osteolytic bone damage. The present study determined the potential of MSC that were unmodified as compared to that genetically engineered to over-express OPG in bone remodeling following osteolytic damage. Results indicated that naïve MSC inhibited tumor growth, comparable to MSC over-expressing OPG by formation of new bone around the tumor cells and by inhibiting osteoclast activation.

MATERIALS AND METHODS

Cell lines and reagents. Osteolytic prostate cancer cell line PC3 expressing firefly luciferase was a generous gift from Dr. Kenneth J. Pienta (University of Michigan, Ann Arbor, Michigan) and maintained in RPMI-1640 medium (Mediatech Inc. Hendron, VA) supplemented with 10% fetal bovine serum (Mediatech Inc.) and penicillin/streptomycin (Mediatech Inc). Osteoblastic prostate cancer cell line C4-2B was a generous gift from Dr. Marco G. Cecchini, Department of Urology and Department of Clinical Research, University of Bern, Switzerland and maintained in T-medium (Invitrogen, Carlsbad, CA) supplemented with 10% FBS and antibiotics. RAW 264.7 cells were obtained from the ATCC (Manassas, VA) and maintained in α-MEM supplemented with 10% FBS, 4 mM L-glutamine and antibiotics. MSC were maintained in Stem Line medium (Sigma-Aldrich Corp. St. Louis, MO), supplemented with 10% FBS, 4mM L-Glutamine and penicillin/streptomycin. HEK293 cells were purchased from ATCC and maintained in DMEM supplemented with 10% new born calf serum and penicillin/streptomycin. Isolation, purification and differentiation of mouse MSC from C57BL/6 mice were carried out as described recently (21). Antibodies for cytokeratin-18 and GFP were purchased from Abcam Ltd. (Cambridge, MA). Secondary immunodetection was performed using anti-rat and/or anti-rabbit ABC kits purchased from Vector Laboratories (Burlingame, CA). Total RNA was isolated using Trizol (Invitrogen, Carlsbad, CA) and purified using a Qiagen mini kit (Valencia, CA). iScript cDNA synthesis kit was purchased from Bio-Rad (Hercules, CA). Primers for RT-PCR analysis were designed using the Primer 3 (version 4.0) software and oligonucleotides were purchased from Integrated DNA Technologies, Inc. (Coralville, IA). cDNA samples were analyzed in Bio-Rad iCycler (Hercules, CA). Three-dimensional PC3 beads were prepared and supplied by Vivo Biosciences (Birmingham, AL). Proliferation of PC3 cells were determined by

Vybrant ® MTT Cell Proliferation Assay Kit (Molecular Probes, Inc. Eugene, OR) as recommended by the manufacturer. Lentivirus encoding shRNA constructs for silencing OPG were designed and supplied by Sigma-Aldrich Corp (St. Louis, MO). Alkaline phosphatase enzyme activity was measured using a commercial kit (Sigma-Aldrich Corp. St. Louis, MO) following manufacturer's instructions. Von Kossa staining was performed to detect calcium deposition following standard protocols (22).

Construction of recombinant plasmid and expression analysis. The recombinant OPG used in this study comprised the ligand-binding domain of human OPG (1-201 amino acids) fused to the Fc domain of human IgG. The OPG.Fc fusion gene was isolated from an adenoviral construct (kindly provided by Dr. Joanne Douglas, University of Alabama at Birmingham, Birmingham, AL) and subcloned into AAV plasmid under the control of CMV/chicken β-actin promoter. Expression of OPG.Fc as a secreted protein from the AAV plasmid was confirmed by transient transfection into HEK293 cells using lipofectamine-2000 reagent (Invitrogen Inc. Carlsbad, CA) and testing the supernatants on SDS-PAGE using a mouse monoclonal antibody against human OPG (Chemicon Inc., Temecula, CA).

Osteoclast assay. MSC were cultured for 2 days at confluency when conditioned media was collected, centrifuged at 4000 rpm to pellet any floating cells, and supernatant stored at -80°C. RAW 264.7 cells were cultured in 6-well culture dishes with 25 ng/ml of RANKL (SIGMA-Aldrich, St. Louis, MO) either in regular medium or MSC conditioned medium for 8 days. The culture medium was replaced every alternate day. After 8 days, cells were stained for tartrate

CCR-09-1938 Revision 1

resistant acid phosphatase (TRAP) to determine the effect of MSC conditioned media on osteoclast formation utilizing a leukocyte acid phosphatase kit (SIGMA-Aldrich, St Louis, MO).

Development of osteolytic bone metastasis model in the mouse. Six-week-old male SCID mice were purchased from the National Cancer Institute-Frederick Animal Production Facility (Frederick, MD). Maintenance of the animals was carried out following guidelines of the Institutional Animal Care and Use Committee (IACUC) and all experimental procedures were approved by the IACUC and the Occupational Health and Safety Department of the University of Alabama at Birmingham. The mice were acclimatized for a week following which 10^5 osteolytic PC3 prostate cancer cells, constitutively expressing luciferase, were implanted in the tibia of right leg (n=30) in 20µl PBS. The left tibia served as control and was injected with only PBS. A 3/10 cc (28 gauge) insulin syringe (BD Biosciences, Franklinlake, NJ) was used for the intra-tibial injection of the prostate cancer cells under isoflurane anesthesia.

Bioluminescence imaging. *In vivo* bioluminescence imaging was conducted in a cryogenically cooled IVIS-100 system (Xenogen Corp., Alameda, CA, USA) to detect luciferase expression using living imaging acquisition and analysis software (Xenogen Corp.) as described (11). For each animal, bioluminescence imaging were performed before, and 4 weeks after the initiation of MSC treatment.   The intensity of light emission was represented with a pseudo color scaling of bioluminescent images.   The bioluminescent images were overlaid on black and white photographs of the mice collected at the same time. Bioluminescence units were converted as counts/second for each animal and final counts were divided by the initial counts and plotted graphically as a measure of tumor growth.

Micro-CT analysis. Superficial CT scanning of whole skeleton was performed on live animals using MicroCAT II (Imtek, Inc. Knoxville, TN). For determination of the 3-D architecture of the trabecular and cortical bones, mice were sacrificed and tibia were harvested and analyzed in an advanced µCT instrument (µCT 40, Scanco Medical AG, Bassersdorf, Switzerland). Two scans were performed on each tibia, one for whole tibial bone with 16 µm resolution and one for trabecular analysis with a 6 µm resolution. For the whole tibia the scan was composed of 1129 slices with a threshold value of 265. A 3-dimensional reconstruction of the images was performed with the region of interest (ROI) consisting of both trabecular and cortical areas. The scan of the trabecular bone was performed below the growth plate. Each scan consisted of 209 slices of which 100 were used for the analysis. ROIs were drawn on each of the 100 slices just inside the cortical bone, to include only the trabecular bone and the marrow. Trabecular bone was set to a threshold at 327 to distinguish it from the marrow. The 3-D reconstruction was performed on the ROI which only contained trabecular bone; no cortical bone was present in these ROIs.

Bone histomorphometry. Soft tissues were fixed in 10% neutral buffered-formalin solution for 48 hours before embedding in paraffin for histological analysis. Bone tissues were decalcified in 0.5 mol/L EDTA in Ca^{2+}- and Mg^{2+}-free Dulbecco's PBS (Cellgro) prior to embedding in paraffin. Six µm longitudinal serial sections were cut from the femur and tibia and stained with hematoxylin and eosin (H&E) or Goldner's trichrome stain to determine the characteristics of tumor growth in the bone and the extent of osteolysis in response to different treatments. TRAP staining was performed on bone sections to determine osteoclast activity. Quantitative

osteomeasurements of bones were performed using an Olympus BX51 microscope and Bioqaunt Image analysis Software (R&M Biometrics, Nashville, TN).

Biomechanical testing. Mice were sacrificed 4 weeks after the MSC treatments, and tibiae were collected and fresh-frozen. Specimens were tested to failure by three-point bending on 858 MiniBionix Materials Testing System (MTS Systems). Stiffness, peak load were calculated from the force displacement data.

Immunohistochemistry. Briefly, 6 μM paraffin sections of tibiae were deparaffinized in xylene, and hydrated through graded-alcohol. Antigen retrieval was performed in citrate buffer, pH 6.0, under steam for 20 min. Sections were cooled to room temperature and endogenous peroxidase was removed using 0.3% H_2O_2 in methanol for 30 min and blocked with 3% goat serum for 30 min. Tissue sections were then incubated with primary antibodies overnight at 4°C. Sections were washed in PBST and again incubated at room temperature with biotin-conjugated goat anti-rabbit/anti-rat secondary antibody for 2 hrs. After washing, sections were incubated with streptavidin-conjugated horseradish peroxidase for 1 hr at room temperature. After another wash with PBST, immunodetection was performed using DAB-H_2O_2 (Vector Labs, Burlingame, CA) and counterstained with hematoxylin.

OPG ELISA. For determination of OPG levels, secreted by the PC3 cells, MSC and MSC-OPG, cells were cultured separately for 72 hours and cell numbers were counted and 100 µl of culture media was subjected to ELISA (ALPCO Diagnostics, Wien, Germany) following

Statistical Analysis. Data were analyzed by one-way analysis of variance (ANOVA). A *Tukey test* was also applied for multiple comparisons wherever applicable. Values provided are the Mean ± SEM and the differences were considered significant if *p<0.05*.

RESULTS

Production of OPG by unmodified MSC and inhibition of osteoclastogenesis. Total RNA was isolated from mouse MSC and converted to cDNA and subjected to real-time PCR analysis. The result indicated expression of OPG mRNA by the MSC (Figure 1A). OPG immunostaining was also performed on cultured MSC, which clearly indicated production of OPG by the MSC (Figure 1B). Ability of MSC to inhibit osteoclastogenesis was tested *in vitro* by culturing pre-osteoclast RAW 264.7 cells in regular medium or MSC-conditioned medium in the presence of RANKL for seven days. TRAP staining indicated significant number of osteoclasts in RAW cells cultured in regular medium, comparable to RAW cells grown in MSC conditioned medium (Figure 1C). Levels of OPG produced in culture as secreted protein by PC3 cells, MSC and MSC genetically engineered to over-express OPG are given in Supplementary Figure 4.

Inhibition of tumor growth by MSC. To determine the effect of MSC in preventing the growth of prostate tumor in the bone, 6-week-old male SCID mice were injected intra-tibially with 10^5 osteolytic human prostate cancer cells, PC3, expressing firefly luciferase. The next day 5×10^5 bone marrow-derived mouse MSC, which were unmodified or over-expressing OPG (MSC-OPG) were injected in the tibia in proximity to the tumor cells. Growth of prostate tumor in the bone was evaluated by bioluminescence imaging four weeks after the administration of the MSC, which indicated almost 90% inhibition of tumor growth in both the treatment groups (Figure 2A&B). MSC-OPG did not show any advantage over unmodified MSC in preventing tumor progression.

MSC therapy is ineffective for end-stage disease. To test if therapy with MSC is effective after the tumor has established in the bone microenvironment with high degree of oseteolytic damage, PC3 cells were injected in the tibia and allowed to grow for 2 weeks. Then, 5×10^5 MSC (unmodified or over-expressing OPG) were injected in the same location. Tumor progression was evaluated 4 weeks after the treatment and bioluminescence imaging indicated inhibition of tumor growth in some of the treated mice compared to the untreated ones, although data was not significantly different (*P>0.05*) between treated and the untreated animals when all the mice were taken into consideration for comparison (Figure 2C). Similar observations were made when histological architecture of the tibia was studied for bone loss due to MSC therapy (data not shown). These data suggest requirement of optimal number of MSC to prevent osteolysis in prostate cancer bone metastasis at an earlier time.

Effect of MSC therapy in bone remodeling: Micro computed tomography (µCT) of the skeleton showed significant loss of bone in the region of implantation of the PC3 cells, whereas complete restoration was observed in the tibiae treated with MSC and MSC-OPG (Figure 3A). Tibiae were harvested from the mice and studies were performed to understand the ultra-structure of the tibia. Three-dimensional µCT data indicated a significant decline in relative bone volume and trabecular connectivity density in untreated mice compared to age-matched normal mice. Both trabecular and cortical bone structures were completely restored in mice with PC3 cells in the tibia by the MSC therapy (Figure 3B). It is interesting to note that the relative bone volume and trabecular connectivity density in the treated mice significantly exceeded that observed in the tibiae of normal mice, indicating the effectiveness of the therapy. Bone restoration was highest in mice treated with MSC-OPG, which may be due to significant

13

inhibition of osteoclastogenesis due to overproduction of OPG as compared to unmodified MSC treated mice (Figure 3B; Supplementary Figure S1 A&B). In MSC-OPG treated mice restoration of tibial bone resulted in limitation of marrow space and might compromise important event(s) like hematopoiesis, hence was excluded in further experiments. Histomorphometry supported the results obtained from bioluminescence imaging and µCT analysis. TRAP staining revealed highest number of osteoclasts in the untreated tibia, mainly at the tumor-bone interface, whereas the number and size of osteoclasts were significantly decreased in the tibia of the treated mice. Both the MSC and MSC-OPG treated mice indicated similar pattern of osteoclast staining (Figure 3C). Three-point mechanical testing of the tibial bone was performed to determine the mechanical strength after treatment. Data indicated similar bone strength in MSC treated mice compared to normal mice tibia (Supplementary Figure S2 A&B).

Interaction between PC3 and MSC *in vivo*. Outcome of the previous experiment suggests that the therapeutic effects of MSC are not highly apparent when administered at the advanced stages of tumor-induced osteolytic bone lesion. It is likely that at a later stage the number of tumor cells in the tibia outnumbered the input MSC. MSC therapy did not influence the prostate tumor growth in the bone in a negative manner, even at later stages. This prompted us to study the interaction between the MSC and the PC3 cells in the bone *in vivo.* 10^5 PC3 cells were injected in the tibia and allowed to grow for 1 week for detectable tumors when 5×10^5 MSC were injected in the same site. MSC used here were derived from a GFP transgenic mouse. Mice were sacrificed 1 week after the injection of MSC and tibiae were harvested and subjected to histomorphometry. Results showed formation of new bone surrounding the tumor nests (Figure 4A). When analyzed under polarized light this newly formed bone comprised of randomly

oriented collagen fibers, called woven bone and characteristic to fracture healing and prostate cancer bone metastasis in human (Figure 4 A&B). Human epithelial cell marker cytokeratin-18 immunostaining was performed to identify the prostate tumors in the bone (Figure 4Cc), which also exposed a multiple layers of fibroblast-like cells arranged in concentric circle separating the tumor cells from the newly formed bone, which also negatively stained for cytokeratin-18. The outermost layer of these fibroblast-like cells were often seen to be embedded or being transformed into the newly formed bone (Figure 4C a&c). These cells stained positively for GFP, which indicated new bone formation in the treated mice formed predominantly from exogenously administered MSC (Figure 4Cd). Formation of new bone around the tumor cells resulted in restricting the growth of prostate tumor cells in the tibia. No such woven bone formation was noticed in tibia injected with MSC in the absence of PC3 cells, suggesting bone formation in the PC3 injected tibia is triggered by the prostate tumor cells (Figure 4A). RT-PCR analysis of mRNA isolated from MSC obtained from a co-culture experiment with PC3 cells for 10 days showed no significant up-regulation of osteogenic genes in the MSC indicating differentiation of MSC towards an osteoblastic lineage may have been driven by osteolysis due to enhanced osteoclastogenesis (Figure 5 A&B). In fact, TRAP staining indicated intense osteoclast activity at the tumor-bone interface (Figure 4Cb).

Characterization of osteoblastic phenotype in prostate cancer bone metastasis. We compared the growth kinetics of highly osteolytic PC3 cells and the osteoblastic C4-2B cells in the tibia of SCID mice. The rate of tumor progression was significantly lower in the tibia injected with C4-2B cells as compared to PC3 cells (Figure 6 A&B). Although PC3 cells induced severe osteolysis by 1 month after inoculation, C4-2B cells produced osteoblastic events by 2

months after administration. There was a gradual switch from osteoblastic to osteolytic phenotype when C4-2B cells were allowed to grow for 6 months in the tibia (Figure 6C). These observations indicate that the growth kinetics of the cancer cells in the bone might be the determining factor favoring osteoblastic or osteolytic outcome.

Role of MSC-produced OPG in bone formation. To test the significance of OPG in this process, an MSC line was generated where OPG expression was silenced using a lentivirus producing shRNA targeting (Supplementary Figure S3). OPG silenced MSC failed to differentiate into osteoblast *in vitro* as determined by von Kossa staining (Figure 1D) and no significant new bone formation was observed in the tibia when these MSC were tested against PC3 cells in a similar experiment mentioned in the previous section (Figure 4A). Moreover, conditioned medium from OPG silenced MSC failed to inhibit osteoclastogenesis when RAW cells were cultured for 8 days in presence of RANKL (Figure 1C), suggesting requirement of OPG for osteoblast differentiation and inhibition of osteoclastogenesis.

Effects of bone marrow microenvironment on the growth of PC3 cells: To test the effects of MSC on the prostate cancer cells, PC3 cells were co-cultured in a 3-dimension matrix with MSC in presence or absence of bone marrow conditioned medium for 3 days. MTT assay was performed to determine cell proliferation. Addition of naïve MSC to the co-culture did not alter PC3 cell proliferation compared to PC3 cultured only in bone marrow conditioned medium. An increase in cell proliferation was noted only when PC3 cells were cultured in bone marrow conditioned media along with MSC over-expressing OPG (*$P<0.001$*; Figure 5C), supporting that OPG is also a survival factor for the prostate cancer cells (23). This suggests that the

inhibitory effect of MSC on the growth of prostate cancer *in vivo* is an indirect effect and

mediated by inhibition of osteoclastogenesis and differentiation into osteoblasts.

DISCUSSION

Results of the present study indicate the therapeutic potential of unmodified MSC in inhibiting the growth of prostate tumor in the bone and prevention of bone loss. MSC did not induce direct apoptosis of tumor cells, instead inhibition of tumor growth in the bone was mediated by new bone formation around them. Although significant therapeutic advantage can be obtained in osteolytic bone metastasis utilizing this approach, absence of a direct killing mechanism may help the metastasis re-establish itself in course of time. The beneficial effects of MSC can thus be further amplified by modifying them *ex vivo* to express tumoricidal genes besides retaining their ability to differentiate into bone. A recent study utilized MSC expressing urokinase-type plasminogen antagonist amino-terminal fragment (hATF) and showed inhibition of tumor growth by inhibiting angiogenesis prevented bone loss (24). Majority of the studies indicated that MSC promote tumor growth by participating in tumor stroma formation and establishment of pre-metastatic niche. Our *in vitro* studies showed an increase in proliferation rate of prostate cancer cells only when co-cultured with the MSC over-expressing OPG. However, the same MSC, over-expressing OPG tested provided a therapeutic effect *in vivo*. Hence, the observed *in vitro* effects could be attributed only to secretory proteins in the co-culture system and may not include other events in the tumor microenvironment. MSC inhibited the growth of prostate tumor in the bone *in vivo* by laying down new bone around the cancer cells, which slowed their rapid growth. Other factors such as cell contact *in vivo* may have also played important roles in addition to the effects of OPG in increasing osteogenesis.

Although the difference in tumor volume between unmodified MSC (MSC-GFP) and MSC over-expressing OPG was not statistically significant, there was an observable difference

in the MSC-GFP group, which showed less tumor growth compared to MSC-OPG group. Since OPG may serve as a survival factor for tumor cells, this observation also indicates the importance of regulated expression of OPG for restoration of bone damage following osteolytic bone metastasis. Further, identification of TRAIL binding and RANK binding domains on OPG would allow genetic modifications in OPG to abolish TRAIL binding.

The present study also highlights the formation of woven bone in osteoblastic metastases (25-27). In our study, the therapeutic effect of the MSC is initially imparted by the woven bone formation surrounding the tumor nests. Formation of woven bone also characterizes osteoblastic metastases in prostate cancer and normal to fracture healing. Roudier et al (2008) performed a detailed histomorphic analysis of bone samples obtained from prostate cancer patients with bone metastasis and observed equal representation of osteoblastic and osteolytic components (2). They also showed that the woven bone formation in the osteoblastic metastases originated from the skeletal mesenchymal stem cells. The pattern of woven bone formation in our experiment truly matches the histological pattern observed in patient with prostate cancer bone metastasis as reported by Roudier et al, 2008. We speculate that the presentation of woven bone in prostate cancer bone metastasis is an endogenous therapeutic response by the resident MSC rather than a pathological outcome. Continuous presence of tumor cells in the bone induces osteolysis which in turn signals the MSC to initiate osteoblastogenesis and manifest the formation of woven bone as part of an early therapeutic response. As we compared growth kinetics of highly osteolytic PC3 cells vs. osteoblastic C4-2B cells in the tibia of SCID mice, the rate of tumor growth is significantly lower in tibia injected with C4-2B cells compared to PC3 cells. Therefore, it is likely that low turnover of C4-2B cells provides a therapeutic window for the endogenous MSC to induce bone formation to make up for the lost bone due to initial osteolytic event required by

the cancer cells to colonize in the bone microenvironment. At this point we are unable to comment on other factors responsible for the slow *in vivo* turnover of the C4-2B cells. When mice were sacrificed 6-months after the implantation of the C4-2B cells, all the lesions in the tibiae were of osteolytic nature. Determination of osteoblastic and/or osteolytic phenotype may be dependent on factors such as growth kinetics of the cancer cells, phenotypic changes of the cancer cells, and events like hypoxia in the tumor microenvironment. Hypoxia is known to promote osteolytic bone metastasis and suppresses osteoblast differentiation (28), therefore slower turnover of C4-2B cells may have delayed the onset of hypoxia compared to PC3 cells, which may have delayed the formation of osteolytic lesions. Nyambo et al reported OPG produced by the bone marrow stromal cells inhibits TRAIL induced apoptosis of the tumor cells and favor growth of prostate cancer *in vitro* (29). Our *in vitro* co-culture assay showed bone marrow microenvironment and OPG produced by the MSC favored PC3 cell proliferation. Interestingly, MSC or MSC-OPG imparted therapeutic benefits when applied *in vivo*. Based on these findings we conclude that primary MSC has the potential to provide therapeutic advantage in limiting the establishment of prostate cancer in the bone at early stage by the virtue of its ability to differentiate into bone and inhibit osteoclastogenesis. These data signify that relatively abundant amounts of MSC in the tumor microenvironment can provide therapeutic effects by activating OPG and/or other factor(s) through interactions with prostate cancer cells. Since the amount of MSC in the bone microenvironment is extremely low (1 in 10^8 cells), strategies to endogenously mobilize and proliferate MSC upon bone metastasis of osteolytic cancers may provide significant therapy and reduce morbidity and mortality encountered in late stage prostate cancer patients. The aim of the present study was to determine potential of adult, bone marrow-derived MSC for the prevention of cancer osteolysis. Based on the limitations of the model used,

20

it is imperative that additional studies should be performed with other osteolytic bone metastasis models having the bone defect in entire skeleton, in imuunocompetent animals, before translating the findings for humans.

ACKNOWLEDGEMENT

FIGURE LEGENDS

Figure 1: **Expression of OPG by MSC and its effects on osteoclast formation *in vitro*.** (A) RT-PCR analysis showing OPG mRNA expression in unmodified mouse MSC. (B) Immunocytochemical localization of OPG in cultured mouse MSC. (C) Pre-osteoclast RAW cells were cultured in MSC conditioned medium in the presence of RANKL for 7 days. TRAP staining indicated inhibition of osteoclastogenesis in RAW cells grown in MSC conditioned medium compared to RAW cells grown in regular medium in the presence of RANKL. Conditioned medium from OPG-silenced MSC (OPG-KO-MSC) failed to prevent osteoclast formation. TRAP, Tartrate resistant acid phosphatase; RM, regular media; CM, conditioned media. (D) Control MSC and OPG-KO-MSC were tested for differentiation into osteoblast lineage using osteoblast medium for 2 weeks. Von Kossa staining was performed to detect calcium deposits (black) to confirm that osteoblast lineage differentiation is compromised in OPG-KO-MSC (right panel) as compared to unmodified MSC (middle panel). There was no positive staining in MSC culture without the osteoblast medium (left panel).

Figure 2: **Tumor growth following MSC therapy**. Non-invasive total body imaging was performed on the day of intra-tibial injection of PC3 cells (day 0) and 4 weeks after the intra-tibial administration of the MSC. (A) Mice represented in the left panel are the same mice that are represented in the right panel and they maintain the same order of alignment. (B) Quantitative analysis of luciferase expression as a measure of tumor growth, 4 weeks after the treatment with MSC or MSC modified to over-express OPG (***P<0.001*). (C) When tumor cells were allowed to grow for 2 weeks followed by administration of MSC, therapeutic benefits are apparent but not statistically significant (*P>0.05*).

Figure 3: **Histomorphometric analysis of bone**. (A) 3-dimensional scanning µCT of the mouse skeleton showing restoration of tibia following MSC therapy compared to untreated mice. (B) 3-dimensional transmission µCT of the bone showing significant osteolysis in the tibia due to the growth of PC3 cells, whereas MSC and MSC over-expressing OPG therapy prevented osteolysis and reduced tumor burden significantly. When compared to normal tibia, both the treated groups demonstrated higher relative bone volume and trabecular bone density. MSC over-expressing OPG treated mice showed the highest bone volume and trabecular density. This is likely due to higher inhibition of osteoclastogenesis. Sections of tibia stained with Goldner's trichrome stain, where mineralized bone stains blue-green as shown in the bottom panel (Original magnification x25). (C) Reduction of osteoclast activity following treatment as determined by TRAP staining. Both MSC and MSC over-expressing OPG demonstrated significantly less osteoclast activity at the tumor-bone interface (arrowheads) as compared to untreated mice. (Original magnification x200)

Figure 4: **Mechanism of tumor inhibition following implantation of MSC in tibiae with PC3 tumors.** (A) Histomorphology of tibia showing presence or absence of new bone formation surrounding tumor nests in mice tibiae following implantation of unmodified MSC only, or following PC3 tumor cell implantation. Polarized light microscopy showing the newly formed bone, composed of randomly-oriented, mineralized collagen fibers (woven bone) (Original magnification x100). When MSC were implanted into a normal tibia without the tumor cells, no such bone formation was observed (far left panel). When PC3 cells were injected in the tibia followed by implantation of MSC (OPG silenced) similarly no significant bone formation (far right panel) was observed suggesting the requirement of OPG for *in vivo* bone formation. (B)

Graph showing the amount of woven bone formed in the tibia after treatment with MSC, OPG-KO-MSC or MSC-OPG. OPG-KO-MSC resulted in least amount of woven bone (*$P<0.001$*) indicating a requirement for simultaneous inhibition of osteoclastogenesis while MSC differentiate into bone. (C) Hematoxylin and eosin (H&E) staining of the tibia showing spindle-like cells of mesenchymal origin bordering the tumor and the new bone (a). Significant osteoclast activity was noticed by TRAP staining at the tumor-bone interface most likely serving as the initiating factor for the MSC differentiation into osteoblasts (b). Immunostaining with the human epithelial marker cytokeratin 18 indicated tumor nests surrounded by the MSC (c). Staining with GFP antibody confirmed that differentiating MSC are of donor origin (d) (Original magnification x20).

Figure 5: Expression of osteogenic genes. (A) MSC were cultured for 10 days in either regular medium or PC3 conditioned medium. Total RNA was isolated, converted to cDNA and analyzed for up-regulation of osteogenic genes. Data showing no significant change in osteoblastic lineage differentiation after MSC were cultured in conditioned media obtained from PC3 cells. BSP, bone sialoprotein; ALP, alkaline phosphatase; Runx2, runt-related transcription factor; OC, osteocalcin; OP, osteopontin (B) MSC cultured in regular medium or PC3 conditioned medium showing equivalent alkaline phosphatase activity, indicating that PC3 cells did not initiate osteoblastic differentiation in the MSC directly. (C) **PC3-MSC in vitro co-culture assay.** PC3 cells were grown on hu-biogel matrix as 3D spheroids and cultured in a 0.8μm pore size transwell plate along with MSC in the lower chamber. After 72 hours the PC3 beads were collected and analyzed by MTT assay for cell proliferation. Data presented here are Mean±SEM (n=12 for each experimental conditions).

Figure 6: (A) Growth kinetics of osteoblastic C4-2B cells in the tibia of SCID mice. (B) Growth kinetics of PC3 cells in the tibia of SCID mice. (C) C4-2B injected tibia showing osteolytic lesions when allowed to grow for 6 months.

Supplementary figure legends

Supplementary Figure S1: (A) Graphical representation of relative bone volume after MSC and MSC-OPG therapy. The data shows significant restoration of bone (**P<0.001*) in the treated animals as compared to untreated mice. (B) Quantitative data showing a significantly higher trabecular connectivity density in mice after MSC therapy (**P<0.001*) when compared to untreated animals. It is interesting to note that both relative bone volume and trabecular connectivity density exceed values obtained from normal, age-matched mice. Data represented here are of the Mean ± SEM.

Supplementary Figure S2: Mechanical strength of the tibial bone. The peak load (S3A) and stiffness (S3B) of tibia following treatment with MSC in PC3 cell implanted groups were found to be statistically similar compared to tibia of age-matched control mice.

Supplementary Figure S3: MSC with targeted knockdown of OPG expression. Immunofluorescence staining showing OPG expression in MSC and MSC with OPG silenced (magnification x200).

Supplementary Figure S4: Quantitative analysis of OPG production from cultures of PC cells, unmodified MSC and MSC over-expressing OPG. The assay was performed in triplicate (*p<0.05*)

REFERENCES

1. Jemal A, Siegel R, Ward E, Murray T, Xu H, Thun MJ. Cancer statistics, CA Cancer J Clin 2007; 57:43-66.

2. Roudier MP, Morrissey C, True LD, Higano CS, Vessella RL, Ott SM. Histopathological assessment of prostate cancer bone osteoblastic metastases. J Urol 2008; 180:1154-60.

3. Ye L, Kynaston HG, Jiang WG. Bone metastasis in prostate cancer: molecular and cellular mechanisms. Int J Mol Med 2007; 20:103-11.

4. Guise TA, Yin JJ, Mohammad KS. Role of endothelin-1 in osteoblastic bone metastases. Cancer 2003; 97: 779-84.

5. Choueiri MB, Tu SM, Yu-Lee LY, Lin SH. The central role of osteoblasts in the metastasis of prostate cancer. Cancer Metastasis Rev 2006; 25: 601-9.

6. Blair JM, Zhou H, Seibel MJ, Dunstan CR. Mechanisms of disease: roles of OPG, RANKL and RANK in the pathophysiology of skeletal metastasis. Nat Clin Pract Oncol 2006; 3: 41-9.

7. Wittrant Y, Theoleyre S, Chipoy M, et al. RANKL/RANK/OPG: new therapeutic targets in bone tumours and associated osteolysis. Biochim Biophys Acta 2004; 1704:49-57.

8. Dougall WC, Chaisson M. The RANK/RANKL/OPG triad in cancer-induced bone diseases. Cancer Metastasis Rev 2006; 25:541-9.

9. Whang PG, Schwarz EM, Gamradt SC, Dougall WC, Lieberman JR. The effects of RANK blockade and osteoclast depletion in a model of pure osteoblastic prostate cancer metastasis in bone. J Orthop Res 2005; 23:1475-83.

10. Simonet WS, Lacey DL, Dunstan CR, et al. Osteoprotegerin: A novel secreted protein involved in the regulation of bone density. Cell 1997; 89: 309-19.

11. Chanda D, Isayeva T, Kumar S, et al. Systemic osteoprotegerin gene therapy restores tumor-induced bone loss in a therapeutic model of breast cancer bone metastasis. Mol Ther 2008; 16: 871-78.

12. Holen I, Shipman CM. Role of osteoprotegerin (OPG) in cancer. Clin Sci (Lond) 2006; 110:279-91.

13. Onyia JE, Galvin RJ, Ma YL, et al. Novel and selective small molecule stimulators of osteoprotegerin expression inhibit bone resorption. J Pharmacol Exp Ther 2004; 309:369-79.

14. Vanderkerken K, De Leenheer E, Shipman C, et al. Recombinant osteoprotegerin decreases tumor burden and increases survival in a murine model of multiple myeloma. Cancer Res 2003; 63:287-9.

15. Zhang J, Dai J, Qi Y, et al. Osteoprotegerin inhibits prostate cancer-induced osteoclastogenesis and prevents prostate tumor growth in the bone. J Clin Invest 2001; 107:1235-44.

16. Morony S, Capparelli C, Sarosi I, Lacey DL, Dunstan CR, Kostenuik PJ. Osteoprotegerin inhibits osteolysis and decreases skeletal tumor burden in syngeneic and nude mouse models of experimental bone metastasis. Cancer Res 2001; 61:4432-6.

17. Capparelli C, Kostenuik PJ, Morony S, et al. Osteoprotegerin prevents and reverses hypercalcemia in a murine model of humoral hypercalcemia of malignancy. Cancer Res 2000; 60:783-7.

18. Kumar S, Chanda D, Ponnazhagan S. Therapeutic potential of genetically modified mesenchymal stem cells. Gene Ther 2008; 15: 711-15.

19. Studeny M, Marini FC, Dembinski JL et al. Mesenchymal stem cells: Potential precursors for tumor stroma and targeted delivery vehicles for anticancer agents. J. Natl. Can. Inst 2004, 96:1593-603.

20. Nakamura K, Ito Y, Kawano Y et al. Antitumor effect of genetically engineered mesenchymal stem cells in a rat glioma model. Gene Ther 2004; 11: 1155-64.

21. Tropel P, Noël D, Platet N, Legrand P, Benabid AL, Berger F. Isolation and characterisation of mesenchymal stem cells from adult mouse bone marrow. Exp Cell Res 2004; 295: 395-406.

22. Kumar S, Ponnazhagan S. Bone homing of mesenchymal stem cells by ectopic alpha 4 integrin expression. FASEB J 2007; 21:3917-27.

23. Holen I, Croucher PI, Hamdy FC, Eaton CL. Osteoprotegerin (OPG) is a survival factor for human prostate cancer cells. Cancer Res 2002; 62:1619-23.

24. Fritz V, Noël D, Bouquet C, et al. Antitumoral activity and osteogenic potential of mesenchymal stem cells expressing the urokinase-type plasminogen antagonist amino-terminal fragment in a murine model of osteolytic tumor. Stem Cells 2008; 26: 2981-2990.

25. Dotan ZA. Bone imaging in prostate cancer. Nat Clin Pract Urol 2008; 5: 434-44.

26. Kingsley LA, Fournier PG, Chirgwin JM, Guise TA. Molecular biology of bone metastasis. Mol Cancer Ther 2007; 6: 2609-17.

27. Guise TA, Mohammad KS, Clines G, et al. Basic mechanisms responsible for osteolytic and osteoblastic bone metastases. Clin Cancer Res 2006; 12: 6213-16.

28. Hiraga T, Kizaka-Kondoh S, Hirota K, Hiraoka M, Yoneda T. Hypoxia and hypoxia-inducible factor-1 expression enhance osteolytic bone metastases of breast cancer. Cancer Res 2007; 67:4157-63.

29. Nyambo R, Cross N, Lippitt J, et al. Human bone marrow stromal cells protect prostate cancer cells from TRAIL-induced apoptosis. J Bone Miner Res 2004; 19:1712-21.

Figure 1A

Marker

OPG

Figure 1B

Control	MSC conditioned medium	MSC-OPG-si conditioned medium

Figure 1C

| Control | Osteoblast medium | OPG-si+Osteoblast medium |

Figure 1D

Figure 2A

Figure 2B

Figure 2C

Naïve	MSC	MSC-OPG

Figure 3A

	Control	Naïve	MSC	MSC-OPG
Whole tibia				
Trabecular area				
Trichrome				

Figure 3B

Figure 3C

| H&E | H&E | Trichrome | Polarized light | H&E |

MSC only   PC3 + MSC   PC3 + MSC-OPG.KO

Figure 4A

Figure 4B

Figure 4C

Figure 5A
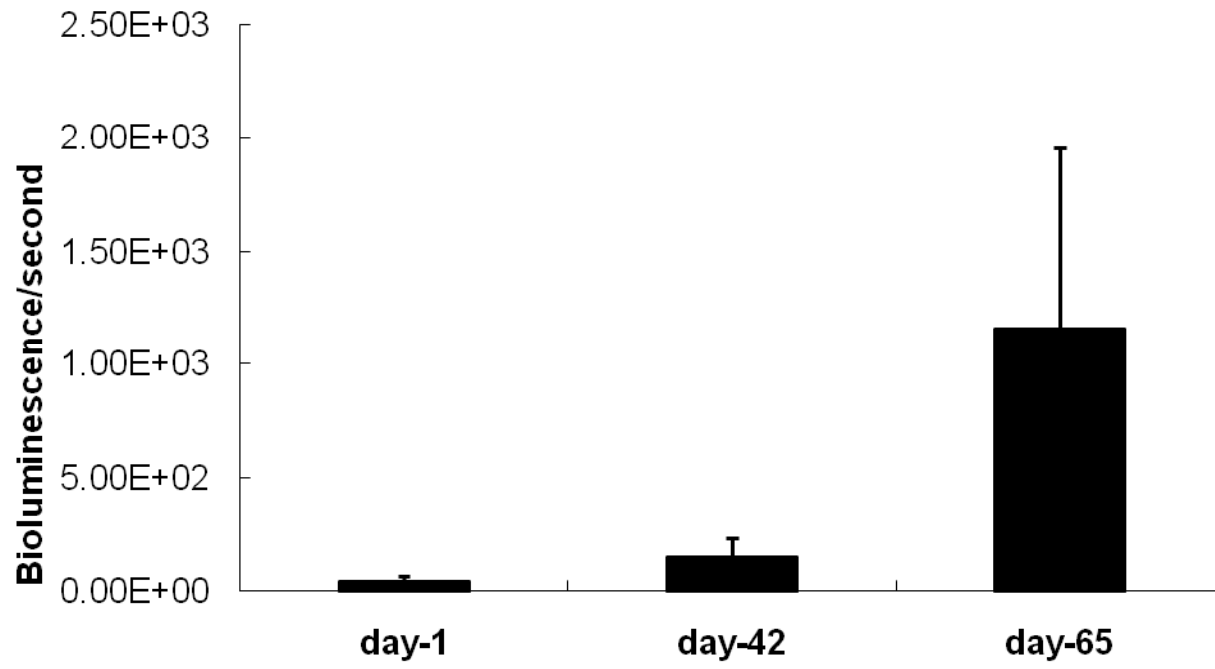
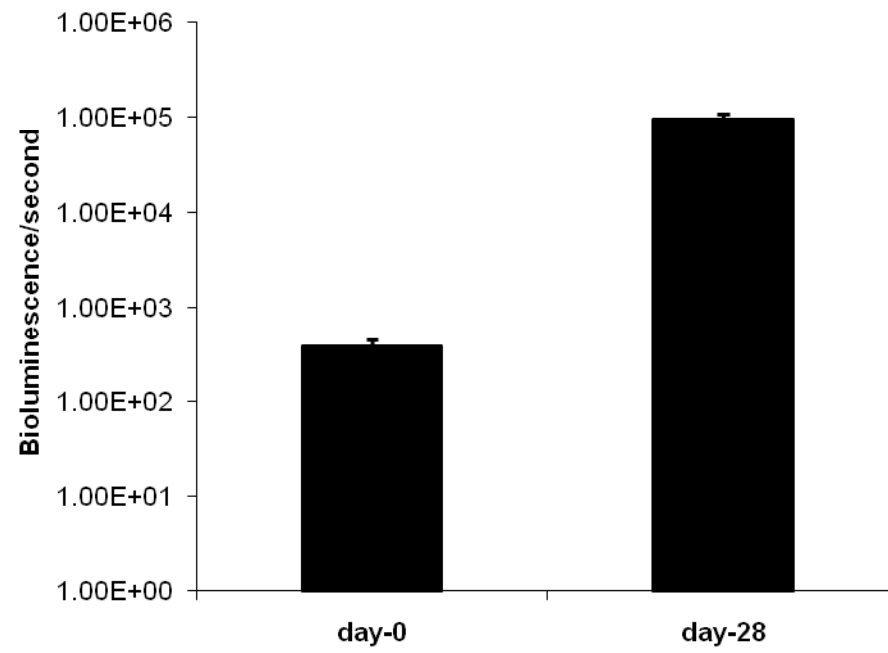**αMEM** **PC3-conditioned medium**

Figure 5B

Figure 5C

Figure 6A
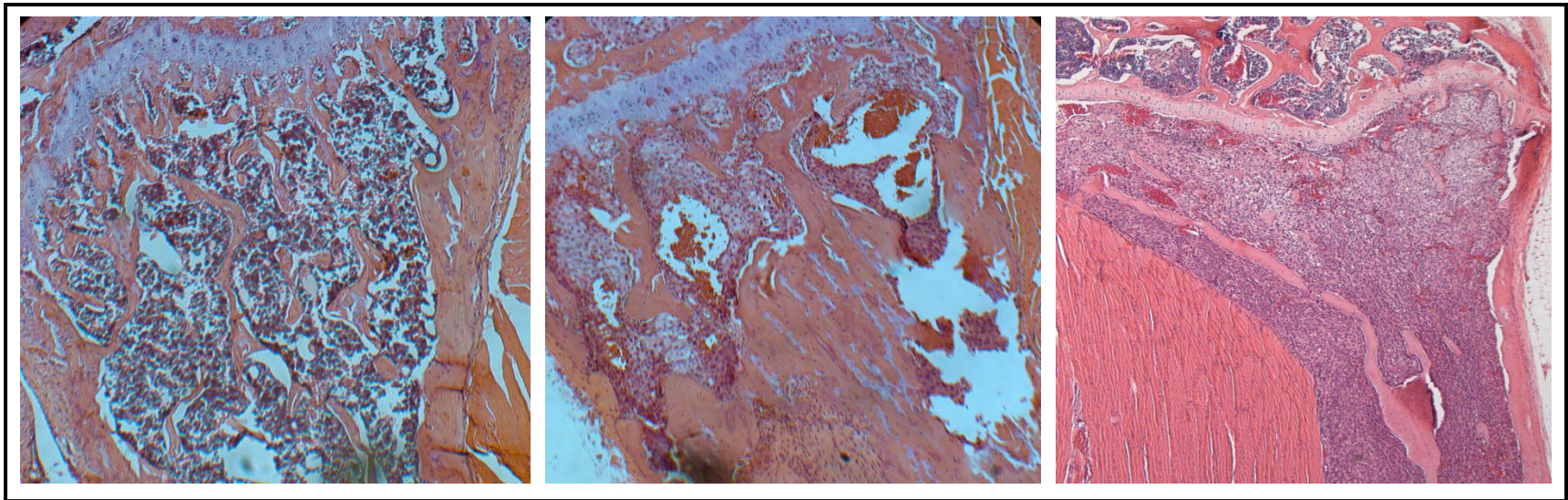
Figure 6B

| Control | C4-2B (2 months) | C4-2B (6 months) |

Figure 6C